

This is the Post-print version of the following article: *Denis Ramón Avellán, José Luis Macías, José Luis Arce, Adrian Jiménez-Haro, Ricardo Saucedo-Girón, Víctor Hugo Garduño-Monroy, Giovanni Sosa-Ceballos, Juan Pablo Bernal, Hector López-Loera, Guillermo Cisneros, Paul W. Layer, Laura García-Sánchez, Gabriela Reyes-Agustín, Víctor Santiago Rocha, Elizabeth Rangel, Eruptive chronology and tectonic context of the late Pleistocene Tres Vírgenes volcanic complex, Baja California Sur (México), Journal of Volcanology and Geothermal Research, Volume 360, 2018, Pages 100-125,* which has been published in final form at: [10.1016/j.jvolgeores.2018.06.012](https://doi.org/10.1016/j.jvolgeores.2018.06.012)

© 2018. This manuscript version is made available under the Creative Commons Attribution-NonCommercial-NoDerivatives 4.0 International (CC BY-NC-ND 4.0) license <http://creativecommons.org/licenses/by-nc-nd/4.0/>

## Accepted Manuscript

Eruptive chronology and tectonic context of the late Pleistocene Tres Vírgenes volcanic complex, Baja California Sur (México)

Denis Ramón Avellán, José Luis Macías, José Luis Arce, Adrian Jiménez-Haro, Ricardo Saucedo-Girón, Víctor Hugo Garduño-Monroy, Giovanni Sosa-Ceballos, Juan Pablo Bernal, Hector López-Loera, Guillermo Cisneros, Paul W. Layer, Laura García-Sánchez, Gabriela Reyes-Agustín, Víctor Santiago Rocha, Elizabeth Rangel



PII: S0377-0273(18)30106-9  
DOI: [doi:10.1016/j.jvolgeores.2018.06.012](https://doi.org/10.1016/j.jvolgeores.2018.06.012)  
Reference: VOLGEO 6406

To appear in: *Journal of Volcanology and Geothermal Research*

Received date: 3 March 2018  
Revised date: 19 June 2018  
Accepted date: 20 June 2018

Please cite this article as: Denis Ramón Avellán, José Luis Macías, José Luis Arce, Adrian Jiménez-Haro, Ricardo Saucedo-Girón, Víctor Hugo Garduño-Monroy, Giovanni Sosa-Ceballos, Juan Pablo Bernal, Hector López-Loera, Guillermo Cisneros, Paul W. Layer, Laura García-Sánchez, Gabriela Reyes-Agustín, Víctor Santiago Rocha, Elizabeth Rangel , Eruptive chronology and tectonic context of the late Pleistocene Tres Vírgenes volcanic complex, Baja California Sur (México). Volgeo (2018), doi:[10.1016/j.jvolgeores.2018.06.012](https://doi.org/10.1016/j.jvolgeores.2018.06.012)

This is a PDF file of an unedited manuscript that has been accepted for publication. As a service to our customers we are providing this early version of the manuscript. The manuscript will undergo copyediting, typesetting, and review of the resulting proof before it is published in its final form. Please note that during the production process errors may be discovered which could affect the content, and all legal disclaimers that apply to the journal pertain.



# Eruptive chronology and tectonic context of the late Pleistocene Tres Vírgenes Volcanic Complex, Baja California Sur (México)

by

**Denis Ramón Avellán<sup>1\*</sup>, José Luis Macías<sup>2</sup>, José Luis Arce<sup>3</sup>, Adrian Jiménez-Haro<sup>4</sup>, Ricardo Saucedo-Girón<sup>5</sup>, Víctor Hugo Garduño-Monroy<sup>4</sup>, Giovanni Sosa-Ceballos<sup>2</sup>, Juan Pablo Bernal<sup>6</sup>, Hector López-Loera<sup>7</sup>, Guillermo Cisneros<sup>2</sup>, Paul W. Layer<sup>8</sup>, Laura García-Sánchez<sup>9</sup>, Gabriela Reyes-Agustín<sup>2</sup>, Víctor Santiago Rocha<sup>10</sup>, and Elizabeth Rangel<sup>9</sup>**

<sup>1</sup>*Cátedras CONACYT – Instituto de Geofísica, Universidad Nacional Autónoma de México, Antigua Carretera a Pátzcuaro 8701, 58190 Morelia, Michoacán*

<sup>2</sup>*Instituto de Geofísica, Universidad Nacional Autónoma de México, Antigua Carretera a Pátzcuaro 8701, 58190 Morelia, Michoacán*

<sup>3</sup>*Instituto de Geología, Universidad Nacional Autónoma de México, Coyoacán 04510, Ciudad de México*

<sup>4</sup>*Instituto de Investigaciones en Ciencias de la Tierra, Universidad Michoacana de San Nicolás de Hidalgo, Morelia, Michoacán*

<sup>5</sup>*Instituto de Geología/Facultad de Ingeniería UASLP, Dr. M. Nava No 5, Zona Universitaria 78240, San Luis Potosí, México*

<sup>6</sup>*Centro de Geociencias, Universidad Nacional Autónoma de México, 76230 Juriquilla, Querétaro*

<sup>7</sup>*División de Geociencias Aplicadas, Instituto Potosino de Investigación Científica y Tecnológica A.C.; Camino a la Presa San José 2055, Lomas 4a Sección, C-P. 78216, San Luis Potosí S.L.P.*

<sup>8</sup>*College of Natural Science and Mathematics and Geophysical Institute, University of Alaska Fairbanks, Fairbanks, AK 99775*

<sup>9</sup>*Posgrado en Ciencias de la Tierra, Instituto de Geofísica, Universidad Nacional Autónoma de México, Coyoacán 04510, México D.F.*

<sup>10</sup>*GEA Alianza para la Exploración Geotérmica, Pera 191, Col. La Huerta, Morelia 58080, MICH, México*

\*Corresponding author e-mail: [denisavellan@gmail.com](mailto:denisavellan@gmail.com)

To be submitted to Journal of Volcanology and Geothermal Research

June 19, 2018

**ABSTRACT**

Based on a detailed geological map and stratigraphy aided by new  $^{230}\text{Th}/^{238}\text{U}$  and  $^{206}\text{Pb}/^{238}\text{U}$  age determinations we established the eruptive chronology of the Tres Vírgenes Volcanic Complex (TVVC). The complex consists of three northeast-southwest aligned stratovolcanoes, which from older to younger are El Viejo, El Azufre, and La Virgen and associated cinder cones and domes. The alignment was fed from fissures that mark the southern trace of the left-lateral Cimarron Fault. The TVVC was built upon the basement rocks of the Peninsular Ranges Batholith (~99 Ma), the Santa Lucia Formation (21.6 Ma), the Esperanza basalt (7.6 Ma), and the 1.1 Ma ignimbrite of El Aguajito caldera. The TVVC began its formation at ca. 300 ka mainly with dacitic lava flows and domes that formed El Viejo volcano ( $4.2 \text{ km}^3$ ). At around 173 ka, activity migrated to the southwest to build El Azufre volcano ( $3.8 \text{ km}^3$ ) with the emission of dacitic lavas and several phases of dome construction and destruction with the generation of pyroclastic density currents. El Azufre's activity ended ~128 ka with the extrusion of the summit dome. At about 112 ka, volcanism migrated 4.2 km to the southwest to begin the construction of La Virgen Volcano through the emission of andesitic and dacitic lavas that built the largest cone of the complex until ~22 ka ( $31.2 \text{ km}^3$ ). This volcano was built upon several stages of cone construction with the emission of lava flows and peripheral dacitic domes and cinder cones. Between 128 and 112 ka six cinder cones vented along the Cimarron Fault between the La Virgen and El Azufre volcanoes. By assuming a constant emission of magma the total volume of the TVVC ( $39 \text{ km}^3$ ) was erupted at an average rate of  $0.13 \text{ km}^3/\text{kyr}$ . Of this volume, effusive eruptions dominated the evolution of the complex (89 %) of which 62% are dacites and 38% andesites. The TVVC rocks have compositions of 50-67 wt. % in silica, and low-medium K (0.5-2.5 wt. %  $\text{K}_2\text{O}$ ). Trace element signatures of the TVVC rocks ( $\text{Sr}/\text{Y} < 40$ ,  $\text{La}/\text{Yb} < 10$ , Nb-Ti negative anomalies and relative enrichments of LILE and LREE) suggest a post-subduction mixture between adakitic and

calc-alkaline magmas. Xenoliths of granodiorites hosted in lavas and La Virgen tephra suggest that magma chambers feeding the complex have stagnated at depths >2 km within the Peninsular Ranges Batholith as confirmed by geobarometry, aeromagnetic data, and the drill-holes of the geothermal field. Today, the Tres Vírgenes geothermal field generates 10 MW of electricity although future exploration of several nearby areas may increase such capacity.

**Keywords:** Tres Vírgenes Volcanic Complex, Cimarron Fault, Baja California, Stratigraphy, Geochronology, Geothermal field

## INTRODUCTION

The Tres Virgenes Volcanic Complex (TVVC) is located about 36 km northwest of the town of Santa Rosalía in the northeastern part of the State of Baja California Sur (Fig. 1). The complex consists of three northeast-southwest aligned volcanoes, which are from older to younger the El Viejo, El Azufre, and La Virgen. The TVVC is the youngest of three volcanic systems in the region, which includes Aguajito (1.17 Ma, Schmitt et al., 2010; Osorio-Ocampo et al., 2016) and Reforma (1.2 Ma, Schmidt, 1975; García-Sánchez et al., 2016) calderas. The TVVC is the site of an active geothermal field operated by the National Power Company (Comisión Federal de Electricidad = CFE). Its exploration began in 1982 with several geological and geophysical studies (i.e. Lira et al., 1997) followed by its exploitation in 1986. During the same decade other authors resumed petrological aspects of the TVVC effusive products (Sawlan, 1984, 1986, 1991; Demant, 1981). During the nineties a new surge of studies presented descriptions of the Plinian rhyolitic eruption of La Virgen volcano (Hausback 1992; Hausback and Sawlan, 1995; Hausback and Abrams, 1996, Capra et al., 1998) along with some geophysical aspects of the complex and the Aguajito caldera (Campos-Enríquez, 1992; Garduño-Monroy et al., 1993). Afterwards,

several studies were dedicated to understand the regional seismicity produced by tectonism, and local seismicity associated to the exploitation of the geothermal field (Romo et al., 2000; Wong, 2000; Wong and Munguia, 2006). After the initial efforts of CFE to produce a general geological map of the TVVC a few studies improved the geology of the region by presenting new geochronological data (Capra et al., 1998; Schmitt et al., 2006; 2010). A need for a new geological map was recognized by CFE who pursued a collaborative project (unpublished internal report DEX-DGL-TV-17) with the Geophysics Institute of the Universidad Nacional Autónoma de México (UNAM) to prepare in a brief time a new general geologic map assisted by  $^{40}\text{Ar}/^{39}\text{Ar}$  geochronology (Macías et al. 2012; Macías and Jiménez-Salgado, 2013). These studies represented a new advance to understand the evolution of the TVVC, however, it lacked detail mapping and stratigraphy because the resolution of the  $^{40}\text{Ar}/^{39}\text{Ar}$  geochronology was diminished by excess argon in the rocks.

In order to understand the stages of construction of the TVVC, its evolution along a NE-SW eruptive fissures, and the types of volcanism associated we carried out additional fieldwork and sampling of eruptive units to refine the geologic map and stratigraphy of the complex. The stratigraphy assisted by new  $^{230}\text{Th}/^{238}\text{U}$  and  $^{206}\text{Pb}/^{238}\text{U}$  geochronology in zircons indicates that the TVVC was built during four stages of construction with different magma emission rates that have not been estimated before. A revision of previous studies and new structural data aids to define the kinematic behavior of the Cimarron Fault and the fissures from which the TVVC was erupted. The analysis of previous seismicity studies (i.e. Antayhua-Vera et al., 2015), new interpretations of aeromagnetic data, lithology of CFE drill holes, granitic xenoliths host in lavas and pyroclastic deposits of the complex, and mineral geobarometry of La Virgen tephra give new insights of location depths of TVVC magmas. Finally, we also present a brief discussion on the chemical affinity of the erupted magmas considering that the complex resides at an unusual

location for the generation of calc-alkaline volcanism in the Peninsula (e.g. Hausback, 1984; Saunders et al., 1987; Capra et al., 1998; Martin et al., 2000; Calmus et al., 2003; Conly et al., 2005; Bellon et al., 2006; Pallares et al., 2007; Negrete-Aranda and Cañon-Tapia, 2008; Germa et al., 2013).

## **TECTONIC AND GEOLOGY BACKGROUND**

The Baja California Peninsula has been the locus of intense tectonism during the Cenozoic. It experienced a major tectonic shift from a subduction setting to a rifting process associated to the opening of the Gulf of California during the middle Miocene (~12 Ma) (Calmus et al., 2003; Conly et al., 2005) (Fig. 1). During the Eocene and Oligocene Baja California was a stable marine shelf that lay west of the active volcanic arc of the Sierra Madre Occidental (Atwater, 1989; Hausback, 1984; Lonsdale, 1991; Stock and Lee, 1994; Martín et al., 2000; Calmus et al., 2003; Pallares et al., 2007). The Sierra Madre Occidental volcanic arc was linked to the subduction of the Farallon plate beneath the North America plate. During late Oligocene and early Miocene, the Farallon plate was subducting eastward underneath the western edge of the North American plate until it was consumed. At that time, the Pacific plate located west of the Farallon plate, came into contact with North America and began to subduct beneath the North American plate. This tectonic regime provoked the development of the Mendocino and Rivera triple point junctions along southern California and northern Baja California (Atwater, 1989; Stock and Hodges, 1989; Calmus et al., 2003). Meanwhile, the subduction of the Pacific plate continued, the Mendocino triple point junction moved northward and the Rivera triple point junction moved southward, lengthening the right-lateral transform plate boundary that had developed between the Pacific and North American plates (Stock and Hodges, 1989; Martín et al., 2000). This right lateral system gave rise to the early stages of the San Andres fault system

(Atwater, 1989; Stock and Hodges, 1989). During this period (between 25 and 11 Ma) the volcanic front migrated towards the west, building the Comodú volcanic arc along the present eastern edge of Peninsula (Martín et al., 2000; Calmus et al., 2003; Pallares et al., 2007; Duque et al., 2015). The progressive extinction of the Comodú arc at ca. 12.5 Ma, is considered to be a consequence of the end of the Pacific-Farallon plate subduction beneath North America plate (Stock and Hodges, 1989; Martín et al., 2000; Pallares et al., 2007). Subduction cessation west of the Peninsula was followed by the opening of the Gulf of California (Stock and Hodges, 1989). This opening occurred first as a Protogulf phase of rifting (between ca. 12-6 Ma) due to the southward migration of the Rivera triple point junction that in addition caused the plate margin to shift from oblique convergence to transtension (Stock and Hodges, 1989). Then a second phase of oblique rifting (ca. 8-6 Ma) occurred when the plate boundary shifted from transtensional faulting to seafloor spreading and transform faulting within the gulf-axis system (Lonsdale, 1989). Between 12.5 and 6 Ma other volcanic centers and magma types in addition to the calc-alkaline arc products were erupted. These volcanic centers migrated westward into the peninsula emplacing high-Mg andesites (e.g., Jaraguay, San Borja, Vizcaino and La Purisima volcanic fields), tholeiitic basalts (e.g., San Ignacio Volcanic Field), adakites (e.g., Santa Clara Volcanic Field) and Nb-enriched basalts (e.g., Santa Clara Volcanic Field). The emplacement of adakites and Nb-enriched basalts has been related to the occurrence of an asthenospheric window possibly linked to the melting of very young oceanic crust from the upper lip of the window and melting of the lithospheric mantle metasomatized by adakitic magmas, respectively (Benoit et al., 2002). Instead, high-Mg andesites likely involved the low degree of melting of adakite-metasomatized mantle containing a sedimentary component caused by the thermal anomaly, as a result of a superficial slab melting (Benoit et al., 2002; Calmus et al., 2003). Tholeiitic basaltic magmas

have been ascribed to the expansion of a slab-free region (Benoit et al., 2002; Negrete-Aranda and Cañón-Tapia, 2008).

The tectonic evolution of the Peninsula continued with a syn-rift period (< 6 Ma) subjected to a transtensional stress regime characterized by sporadic but persisting Pliocene-Quaternary calc-alkaline magmatism (e.g., TVVC, Aguajito and La Reforma calderas) (Saunders et al., 1987; Calmus et al., 2003; Pallares et al., 2007; Negrete-Aranda and Cañón-Tapia, 2008). Nevertheless, during late Quaternary, diverse magma compositions have been erupted as tholeiitic basalts (e.g., Isla San Luis and Isla Tortuga) related to the opening of the Gulf of California, and OIB-type mafic alkaline lavas (e.g., San Quintin Volcanic Field) related to intraplate-type magmatism that occurred after the subduction of the ancestral EPR (Saunders et al., 1987; Calmus et al., 2003; Bellon et al., 2006; Negrete-Aranda and Cañón-Tapia, 2008).

## STRATIGRAPHIC SUCCESSION

A simplified geological map of the studied area is shown in figure 2 supported by seven  $^{230}\text{Th}/^{238}\text{U}$ , and one  $^{206}\text{Pb}/^{238}\text{U}$  in zircons new dates (Appendix 1; Tables 2 and 3) of the different units are resumed in the refined stratigraphic column of figure 3. The stratigraphic succession was grouped into four stratigraphic units belonging to the local basement that are the Peninsular Ranges Batholith, Santa Lucia Formation, Esperanza Basalt, and the Aguajito Caldera. The youngest succession of rocks (Tres Vírgenes Volcanic Complex) consists of 19 volcanic units of Late Pleistocene age (Fig. 3). The summarized stratigraphic succession from base to top consists of:

### **Peninsular Ranges Batholith (PRB)**

The basement of the studied area is made of plutonic rocks of the Peninsular Ranges Batholith (PRB) (Gastil, 1975; Silver and Chappell, 1988; Kimbrough et al., 2001; Kimbrough et al.,

2014). Silver and Chappell (1988) and Kimbrough et al. (2001) described the *PRB* as an 800 km long intrusive from southern California to the Vizcaino peninsula in central Baja California. In the vicinity of the study area, intrusive rocks crop out inside and outside the Reforma caldera (Schmidt, 1975). Here, light-pink, 10-15-cm wide, aplite dikes intrude the batholith. Dark-gray aphanitic diabase dikes ( $\geq 1$  m in width) transect the batholith and sometimes appear similar to the ring-dikes related to the caldera fault. In the Tres Vírgenes geothermal field the batholith was drilled at a depth of 1,129 m below the surface in the LV-2 exploratory well of CFE (Fig. 2) (Garduño-Monroy et al., 1993). Hand specimens of the batholithic rock have a pinkish-white and rarely greenish-gray color. Some deposits as La Virgen Tephra contains rounded granodioritic xenoliths from the assimilated underlying pluton. An  $^{40}\text{Ar}$ - $^{39}\text{Ar}$  age of mineral biotite from a granitic enclave, collected within the Tres Tortugas lava dome, located ca. 10 km south of La Virgen volcano yielded a plateau age of ca.  $99.1 \pm 0.8$  Ma (Macías et al., 2012). This age agrees with U-Pb zircon dates of La Posta type plutons ranged between 92 and 99 Ma (Kimbrough et al., 2001; Kimbrough et al., 2014).

### **Santa Lucia (SL)**

In the Tres Vírgenes area the rocks belonging to the Comondú group (e.g. Hausback, 1984; Sawlan and Smith, 1984; Sawlan, 1991; Martín et al., 2000) are exposed at the Sierras of San Francisco to the northwest and Sierra Santa Lucia to the south (Fig. 2). Because its proximity to the TVVC, we describe the Santa Lucia rocks in this study. The Santa Lucia Range has peneplain and hogback landforms. This unit crops out at the El Mezquital and Cuesta Vieja locations along the Campamento Fault scarp covering a surface of ca.  $29 \text{ km}^2$  with thicknesses varying from 140 to 360 m. The Santa Lucia stratigraphic unit was described in the geothermal exploration drill-hole LV2 of Comisión Federal de Electricidad where it is 364 m thick and overlies the PRB. At the Campamento Fault scarp, *SL* typically appears as massive or chaotic beds with subrounded



and angular lava fragments embedded in a welded fine ash matrix (section 94; Fig. 2). In this work, we obtained a new  $^{206}\text{Pb}/^{238}\text{U}$  zircon age of  $21.59 \pm 0.29$  Ma that is consistent with its stratigraphic position and in agreement with previous studies (Table 1; Fig. 4).

### **Esperanza Basalt (*EB*)**

Originally, Sawlan and Smith (1984) assigned the name Esperanza basalt to the tholeiitic basalts exposed in northern Baja California Sur. Germa et al. (2013) named these tholeiitic basalts as the San Ignacio volcanic field.

In the studied area, the *EB* unit crops in the southwestern and southern parts of La Virgen volcano (Fig. 2). The *EB* covers the SL unit and has a flat-surface top. In section 41, it appears as a single massive bed with large vesicles, showing crude near vertical columnar jointing covered by Virgen Tephra (Capra et al., 1998). Previous studies reported ages between 12.5 and 6 Ma for these tholeiitic basalts (e.g., Saunders et al., 1987; Calmus et al., 2003; Conly et al., 2005; Bellon et al., 2006; Pallares et al., 2007). Macías et al. (2012) obtained a  $^{40}\text{Ar}/^{39}\text{Ar}$  whole-rock age of  $7.64 \pm 1.16$  Ma which is consistent with the age range obtained in previous studies.

### **Aguajito caldera (*Ag*)**

Garduño-Monroy et al. (1993) described the Aguajito ignimbrite in association with the evolution of the Aguajito resurgent caldera. The *Ag* unit consists of a dacitic ignimbrite, covered by dacitic domes (Garduño-Monroy et al., 1993). In the studied area *Ag* is exposed to the northern and northeast parts of the TVVC (Fig. 2). Inside the El Azufre gully, *Ag* unconformably overlies Tertiary rocks (e.g., sandstones and carbonate rocks) and pepperitic lavas (Sections 95 and 96; Fig. 2). Here, *Ag* is overlain by the El Viejo Volcano units as well as in other sections 92 and 93 (Fig. 3). Southeast of La Virgen volcano, *Ag* forms a hilly morphology. South of the Aguajito caldera, *Ag* has a tongue-like morphology with high plain landforms or mesas. Garduño-Monroy et al. (1993) reported an age of  $0.76 \pm 0.06$  Ma for the ignimbrite and  $0.5 \pm 0.04$  Ma for post-

caldera domes with the K-Ar method. Schmitt et al. (2006) reported a more precise age of  $1.17 \pm 0.07$  for the ignimbrite (Ag unit) with U/Pb in zircons.

## **Tres Vírgenes Volcanic Complex**

### ***El Viejo lava cone (Vlc)***

El Viejo is the oldest volcano of the TVVC located at the northern tip of the complex (Fig. 2). It overlies the Aguajito ignimbrite and underlies the El Azufre stratocone. Its distribution and stratigraphic position indicate that El Viejo products were erupted southwest of El Aguajito Volcanic Complex. The El Viejo is asymmetrically distributed with a hogback-dome morphology elongated in a NE-SW direction. The volcanic edifice was built predominantly by a stack of three dacitic lava domes that covers an area of ca.  $10 \text{ km}^2$  reaching an elevation of 1,360 m above sea level (Figs. 3). The edifice is truncated on its northeastern flank at the contact with the Ag unit along the El Azufre Fault. These lava domes are typically massive with a mottled structure due to abundant enclaves (e.g., sections 75, 83 and 91). A debris avalanche deposit is exposed at section 82 showing shattered lava blocks with a coarse ash matrix (Vda, Fig. 2). The absolute age of the oldest lava dome is unknown, but based on its stratigraphic position it is older than  $245 \pm 39 \text{ ka}$  according to an  $^{40}\text{Ar}/^{39}\text{Ar}$  whole rock age obtained in the youngest lavas of the volcano (Macías et al., 2012).

### ***El Azufre stratocone (Az)***

The El Azufre stratocone (1,670 m) is located southwest of the El Viejo lava cone (Fig. 2). The edifice was constructed by a thick sequence of block-and-ash flow deposits on its flanks and a steep summit dome (Fig. 3). El Azufre cuts discordantly the El Viejo volcano. The pyroclastic flow deposits form fans distributed to the northwest and southeast of the volcano. These fans are dissected by radial drainage and their bases limit alluvial fans composed of debris flow deposits. One lava sample taken near the top of the El Azufre stratocone yielded a  $^{230}\text{Th}/^{238}\text{U}$  zircon model

age of  $154 \pm 32/-25$  ka (section 04; Table 2; Fig. 5). Another lava sample collected on the southeastern flank of the El Azufre volcano (section 01; Table 2; Fig. 5) yielded a  $^{230}\text{Th}/^{238}\text{U}$  zircon model age of  $146 \pm 27.8/-22$  ka. These ages are consistent with  $^{40}\text{Ar}/^{39}\text{Ar}$  ages obtained for the El Viejo cone of  $<245 \pm 39$  by Macías et al. (2012).

### ***La Virgen scoria cones (Vsc)***

Six scoria cones are distributed around the La Virgen volcano (Fig. 2) (Avellán et al., 2018). These scoria cones are partially covered by younger deposits of La Virgen volcano. Three of these scoria cones lie directly above the southwestern flank of the El Viejo and El Azufre volcanoes and partially underlie to lava flows of La Virgen volcano. These cones coalesce into N-S elongated landforms. Another scoria cone lies northeast of the La Virgen volcano overlying the *Ag* unit and partially underlying two lava flows of La Virgen volcano and debris flows from the Azufre volcano. The remaining two scoria cones are located at the southern and southwestern flanks of the La Virgen volcano. They overlie the *EB* unit and underlie the lava flows of the La Virgen volcano.  $^{40}\text{Ar}/^{39}\text{Ar}$  and  $^{230}\text{Th}/^{238}\text{U}$  zircon geochronology analysis were unsuccessful due to the very low percentage of radiogenic argon and the absence of zircon crystals respectively, for samples from each of these scoria cones.

### ***La Virgen stratovolcano (Vst)***

La Virgen stratovolcano is a symmetrical cone located at the southwestern end of the TVVC (Fig. 2). It has a maximum elevation of 1,940 m above sea level and covers an area of  $59.3 \text{ km}^2$ . This stratovolcano is highly dissected by deep erosion on its western and northwestern flanks. The main edifice is built by at least 12 andesitic to dacitic lava flows and dome units. Their lava flow units radially extended from the central edifice and overlie most of the older units (e.g., *SL*, *EB* and *Ag*). These units form a stack of bedded massive lava flows with poorly developed entablature structure and marginal autobreccias that frequently present tongue-lobate morphology

delimited by levées. Instead, lava domes are confined to the southwestern and southeastern lower flanks of La Virgen volcano where they cover unconformably the *EB* unit. The domes have asymmetric lobate morphology with moderate to high relief and a surface ranging from smooth to blocky. A lava rock sample of the lowermost unit (section 61, Figs. 2 and 3) of La Virgen stratovolcano was dated at  $112 \pm 26/-21$  ka with the  $^{230}\text{Th}/^{238}\text{U}$  zircon method (Table 2; Fig. 5), which is consistent with its stratigraphic position. Other four units yielded modeled zircon ages of  $103.8 \pm 12/-11$  (section 53),  $61 \pm 7/-6.7$  (section 21),  $51 \pm 8.7/-8$  (section 47), and  $41 \pm 6/-5.8$  ka (section 37A) (Table 2) obtained by  $^{230}\text{Th}/^{238}\text{U}$  zircon geochronology that are consistent with their stratigraphic position. The following unit is the La Virgen Tephra (VT), a thick pyroclastic fall deposit emplaced by a Plinian eruption (Capra et al., 1998). Based on their isopach and isopleth maps dispersed to the southwest Capra et al. (1998) concluded that VT originated at a site on the southwest flank of the La Virgen volcano. The VT is widely exposed to the south and southwest sectors of the studied area mantling the Santa Lucia, Esperanza Basalt, and older units of la Virgen stratovolcano. According to their distribution and stratigraphy VT spread out ca.  $500 \text{ km}^2$ , and has a minimum volume of  $1.14 \text{ km}^3$ , and it was preceded by a vulcanian eruption that produced pyroclastic surge and fallout deposits named El Mezquital deposit (Capra et al., 1998). Capra et al. (1998) reported a C-14 age of 6.5 ka BP of a charcoal found at the base of the deposit. Later, Schmitt et al. (2010) combined U-Th and (U-Th)/He zircon dating of a pumice sample obtaining an age of  $30.7 \pm 1.8/-1.4$  ka. This age discrepancy resulted in a discussion of the Plinian event dating (Capra et al., 2007; Schmitt et al., 2007). Our new stratigraphy indicates that the age obtained by Schmitt et al. (2010) may be closer to the expected age of the tephra fall. The youngest unit of La Virgen stratovolcano are a series of black lava flows dispersed around the cone and dated between  $22.0 \pm 2.5$  and  $25.5 \pm 4.4$  ka by Schmitt et al. (2010).

## WHOLE-ROCK COMPOSITIONS

Overall, samples of the TVVC range from high-silica basalts to dacites (49.9-66.7 SiO<sub>2</sub> wt. %) (Fig. 6A; Table 3), with andesitic-dacitic compositions as the dominant rock. La Virgen volcano comprises rocks representing a wider compositional range than El Azufre and El Viejo volcanoes which are constructed by less voluminous lavas of dacitic composition. The TVVC has low-medium K rocks (0.5-2.5 wt. % K<sub>2</sub>O; Fig. 6B) with high concentrations of LILE and LREE, when compared to HFSE and HREE (Fig. 6C-D), overall low Sr/Y (<40, although few samples are 50-65), low La/Yb (<10), low Nb (<6 ppm), and low MgO (<6 wt. %) concentrations (Table 3).

In addition to the TVVC rocks, we analyzed enclaves hosted in lavas (56-59 SiO<sub>2</sub> wt. %), and some regional rocks as lava flows, ignimbrites of the Santa Lucia unit (61.8-72 SiO<sub>2</sub> wt. %), a mafic fissural lava flow (57.7 SiO<sub>2</sub> wt. %), and intrusive rocks of the geothermal exploration drill-hole LV-2 (57.5-61.1 SiO<sub>2</sub> wt. %). The enclaves, ignimbrites, the fissural lava and the intrusive rocks yield similar trace element variations as the TVVC rocks. MgO content show a negative correlation when plotted vs SiO<sub>2</sub>, with the scoria cones and enclaves having the higher content.

We inspected the compositional variability of the TVVC rocks as a function of age (Fig. 6E). The oldest structure of the TVVC is El Viejo volcano, and is formed by dacitic rocks (ca. 300-245 ka). Though El Azufre rocks are younger than El Viejo, but they have the same bulk composition. A series of scoria cones exposed on the N, NE and SW flanks of the La Virgen volcano are mostly mafic than the TVVC rocks. Their chemical composition represents a drastic drop in silica content when compared to previously erupted rocks. La Virgen cone that was built after this mafic pulse progressively erupted silica-rich products (55-66 SiO<sub>2</sub> wt. %), including the La Virgen Tephra (Capra et al., 1998) up to the construction of the upper part of the cone with

andesitic lavas (55-57 SiO<sub>2</sub> wt. %). Overall, Yb, Y, and Nb do not reflect any systematic variations with time. Sr increased after the construction of El Azufre stratocone after which it consistently decreases through time until the emission of the 22 ka lavas, with the exception of some scoria cones that show a clear enrichment in this element.

The trace element signatures (Sr/Y <40, La/Yb <10, Nb-Ti negative anomalies and relative enrichments of LILE and LREE) (Fig. 6 and Table 3) suggests that the TVVC magmas are a mixture of adakitic (La/Yb>20, Sr/Y>50), and calc-alkaline melts. The origin and magmatic processes recorded on the TVVC rocks will be explored in detail in a forthcoming contribution.

## **BASEMENT ARCHITECTURE**

To understand the internal structure of the basement we carried out a review of previous studies, the analysis of morphostructures, the mesostructural geometry of faults, field description of major faults, and the processing and interpretation of airborne data. The TVVC region exposes regional faults that affect the basement and that have controlled the location and distribution of younger volcanic units as describe next.

### **Morphostructural data**

The area was divided in five blocks that have distinctive morphological features arranged in NNE-SSW, and NW-SE orientations as observed in figure 7A: 1) The Aguajito caldera (<1.1 to 0.5 Ma Schmitt et al., 2006, 2010; Garduño-Monroy et al., 1993) lacks a well-defined caldera collapse crater but shows a series of rhyolitic domes disposed in a semicircular way that may evidence the likely caldera edge (Garduño-Monroy et al., 1993). This structure has an elevation of ca. 1,100 m with a deep dendritic drainage and is affected by faults such as the Cimarron Fault and secondary structures. 2) The TVVC (ca. 300 to 22 ka) constituted by three NE-SW aligned peaks (El Viejo, El Azufre, and La Virgen) each one flanked by radial volcanoclastic fans. 3) The

Reforma range is a resurgent caldera with a 10-km semi-circular collapse crater (Garduño-Monroy et al., 1993; Demant, 1981 and 1984; Demant and Ortlieb 1981). Reforma is limited to the SW by the Reforma Fault (Fig. 7B) and to the west by normal faults linked to the tectonics of the Gulf of California. 4) The Santa Lucia Range (800 m; 11 - 25 Ma) forms a NW-SE structural high that is limited to the east by the El Campamento Fault and to the west by secondary and parallel faults to the Mezquital Fault (Garduño et al., 1993). These structural features are linked to trellis and parallel drainage pattern in the range. 5) The San Francisco Range (700 m) forms a NW-SE structural high delimited to the SW by the Mezquital Fault and to the NE by the San Francisco Fault (Garduño et al., 1993). The range presents dendritic, parallel and lattice drainage patterns; the latter linked to the faults that affect it.

### **Description of major faults**

In this study we describe eight structural stations (S1-S8) shown in figure 8. Five main faults bound the five morphological blocks that have contributed to the morphostructural evolution of the zone (Fig. 8A-B). These faults are: 1) The Campamento Fault: a normal fault with a right-lateral component and a high angle escarpment that generates a vertical drop higher than 200 m (Figs. 7C). This N47°W structure dips to the NE. 2) The Mezquital Fault: a normal fault with a right-lateral component and a scarp of circa 150-200 m. This N48°W structure dips to the SW. The genesis of these faults is related to the opening of the Gulf of California. 3) The Bonfil Fault: a right-lateral strike-slip fault with a slight normal component (Fig. 7D). This N25°W structure dips to the SW, has a horizontal displacement of ca. 400 m, and a vertical escarpment of ca. 100 m. This fault shows morphological evidence of recent activity because it controls the course of some river channels, cuts and displaces recent volcanic cones, and sedimentary units. 4) The Reforma Fault: a right-lateral strike-slip fault with a gentle escarpment of ca. 50 m. Its surficial expression consists of several NW-SE segments of right-lateral faults with a relay geometry.

These structures have a little vertical component with visible metric displacements but their total vertical and horizontal displacement is not evident. This fault is covered by young sediments and recent volcanic products, and might be linked to the tectonics of the Gulf of California. 5) The Cimarron Fault: a NNE-SSW structure that dissects the Aguajito caldera and controls the drainage pattern forming a 300 m deep canyon. The horizontal and vertical displacement of this structure is not evident. This fault is segmented at the El Azufre canyon, but its trace continues towards the SSE, controlling the location and the emplacement of the TVVC structures along an eruptive fissure (El Viejo, El Azufre, and La Virgen volcanoes).

### **Mesostructural geometric data**

The mesostructural scale analyses was carried out to understand the geometric characteristics of fractures and faults linked to the Cimarron, Campamento, and Reforma faults. North of the TVVC we collected data at S1, S4 and S5 structural stations where three main fault directions were identified: NNE-SSW, NE-SW, and NW-SE (Fig. 8A-B). The first two, correspond to the Cimarron Fault while the last one is parallel to the Gulf of California faults. The NW-SE fault planes have dips mainly between  $60^{\circ}$  and  $90^{\circ}$ , and in a smaller proportion between  $10^{\circ}$  and  $30^{\circ}$ . Instead, on the footwall of the Campamento Fault (S2), the structures have a NW-SE preferential orientation with dips between  $70^{\circ}$  and  $90^{\circ}$  that are synthetic and antithetic to the main fault. At site S3 the NW-SE structures have  $60$ - $90^{\circ}$  dips. However, some Miocene rocks of the Santa Lucia Range are cut by these faults with dips between  $50$  and  $60^{\circ}$ . In the eastern area (S6, S7, and S8) faults and fractures were grouped into four sets: NNE-SSW, NE-SW, NW-SE, and NNW-SSE. The first three sets are high-angle structures with  $60$ - $90^{\circ}$  dips in agreement with the Infierno canyon and the Reforma Fault. The NNW-SSE planes have dips between  $60^{\circ}$  and  $80^{\circ}$ .

The structural analysis of all these elements at different scales shows a clear correlation between the main fault planes, the mesostructural fractures, and the focal mechanisms reported (Wong et



al., 2006; Antayhua-Vera et al., 2015). All these elements define the geometry in blocks of the area and the current stress regime (Fig. 8B) with blocks bounded by regional faults with best morphological expression.

### **Aeromagnetic data**

We analyzed aeromagnetic data of the Mexican Geological Survey (SGM, 2000). The data was re-processed by using the Geosoft Oasis-assembly software and the Reduction-to- the Magnetic Pole (Baranov and Naudy, 1964) obtaining a residual magnetic field map. With this information, we applied different filters as the Vertical Derivative of the first and second order (Henderson and Zietz, 1949) and Upward Continuations (Henderson, 1970) to highlight subsurface geological features within the contour map of interest. From these data we calculated the depths of the magnetic source in the region between 1.7 km (min) and 2.4 km (max) (Spector and Grant, 1970) with respect to the maximum height of TVVC (Fig. 9). The AS-filter shows two well-defined higher magnetic values in the TVVC peaks than its surrounding area. The magnetic source to the south is related to La Virgen volcano whereas the northern source is related to the El Azufre and El Viejo volcanoes, sites of geothermal exploitation. The La Virgen source can be modelled as a ~4.8 km wide zone in an E-W direction, and ~3 km in a N-S direction, occupying an area of ca. 14 km<sup>2</sup> with a magnetic susceptibility between 0.25 and 0.48 nT/m. The magnetic source of El Azufre and El Viejo volcanoes can be modelled with a body extending ~4.7 km in a NE-SW direction and ~3.3 km in a NW-SE direction, occupying an area of 15.5 km<sup>2</sup> with a magnetic susceptibility between 0.25 and 0.44 nT/m. The two higher magnetic sources are separated by a zone of weakness, probably associated with a NW 45° trending fault (e.g., Campamento Fault) between La Virgen and El Azufre volcanoes. The analysis of the mathematical algorithm of the First Vertical Derivate shown in the contour map of figure 9 indicates that El Azufre and El Viejo volcanoes are also separated by a steep gradient interpreted

as a weakness zone in a NW-SE direction. The contour map of AS shows the existence of positive magnetic anomalies located E-SE of El Azufre volcano and E-NE of the La Virgen volcano that may be related to the thick piles of mafic and intermediate rocks at depth within the basement that might be the suppliers of the thermal source for power generation.

## DISCUSSION

### Tectonic context

The study area is transected by NW-SE faults (e.g. Campamento and Reforma faults) (Fig. 8A-B). These faults behaved as normal faults with dipping blocks to the NE, and with NE-SW conjugate faults (e.g., Cimarron Fault). These faults coincide with the strike-slip fault systems associated to the opening of the Gulf of California that probably correspond to the prolongation of the Guaymas basin structure (Fig. 1). In this tectonic setting, the NNE-SSW Cimarron Fault likely acts as an R' Riedel shear. This structural arrangement is consistent with experimental and theoretical models of wrench tectonic faults carried out by Wilcox et al. (1973) and known as the Riedel shear pattern (Davis et al., 2012). This structural geometry indicates that these faults formed under the same N-S compressional regime with an E-W extension. This is in agreement with the regional transtensional stress field of the right-lateral strike-slip transform fault system of the Gulf of California that has a NW-SE trend (e.g., Angelier et al., 1981; Wong and Munguia, 2006; Antayhua-Vera et al., 2015).

Seismicity in the area suggests that the same tectonic regime operates at present (e.g., Angelier et al., 1981; Wong and Munguia, 2006; Antayhua-Vera et al., 2015). Antayhua-Vera et al. (2015) analyzed 423 local earthquakes (between 0.1 and 2.9 Mc) that occurred from 2003 to 2012 and concluded that these events are concentrated at depths between 0.2 and 7.4 km, located on rocks of the ~90 Ma Peninsular Ranges Batholith and overlying volcano-sedimentary formations.

Seismic stress inversion is consistent with the structural arrangement mentioned above, and the regional tectonic stress field (Antayhua-Vera et al., 2015). In this case, the antithetic left-lateral strike-slip fault (Cimarron Fault System) is associated with a shear zone where the compressional stress is NNW-SSE and the extensional stress is ENE-WSW (Fig. 8A-B). The Cimarron Fault System has been active through the Upper Pleistocene, controlling the volcanic evolution in the area (e.g., location of Aguajito caldera) and NE to SW progression of the TVVC volcanism through time.

### **Geophysical evidences of magma sources**

The TVVC has experienced seismic swarms in 1993 (Wong and Munguia, 2006) and continuous seismicity associated to exploitation of the geothermal field (Lermo et al., 2010; Soto-Peredo and Lorenzo-Pulido, 2012; Antayhua-Vera et al., 2015) that occurred beneath the central part of the complex at depths between 0.2 and 2.5 km. These depths are consistent with circulation of geothermal fluids through fractures associated with the geothermal reservoir (Lermo et al., 2010; Soto-Peredo and Lorenzo-Pulido, 2012). The geothermal exploration drill-hole LV-2 of Comisión Federal de Electricidad reached the PRB at depths of 1.129 km, thus, seismic swarms occurred in fractures developed in the Cretaceous granodiorite and the uppermost volcano-sedimentary units.

Pre-eruptive temperatures and pressures calculated from Fe-Ti oxide pairs and amphiboles of La Virgen rhyolitic tephra pumice suggest that this magma stagnated at depths between 7 and 9 km below the summit at temperatures between 900-930°C (Macías et al., 2012), within the Cretaceous granodiorites. This assumption is supported by common granodiorite xenoliths found in deposits of scoria cones, the Tortugas lavas, the Aguajito ignimbrite, the Virgen Tephra fall deposits, xenocryst populations of zircons found in the  $^{230}\text{Th}/^{238}\text{U}$ -zircon analysis, and xenocrystic zircon with degassed radiogenic He (Schmitt et al., 2006).

A 3D aeromagnetic model reveals that the TVVC magnetic patterns lack any correlations with topography (Fig. 10). Instead, the magnetic anomalies correspond to the prolongation of the Campamento and Reforma fault systems to the NW (Figs. 8 and 9) which follow a NW-SE trend approximately parallel to major regional structures. The central domains under the volcanoes have high magnetic intensities, likely related to the occurrence of shallow magma reservoirs and/or possible discontinuities beneath the volcanoes, linked to sills and dike swarms systems that intruded the Cretaceous Batholith following major faults (Fig. 10).

### **Volcanic Evolution**

During the early Miocene, before the formation of the TVVC, there was an intense volcanic activity in the study area that gave place to thick pyroclastic density current sequences, forming the 21.6 Ma Santa Lucia Range to the south and the contemporaneous San Francisco Range to the west-northwest. These volcanic sequences are part of the Comondú volcanic arc, originated by the Farallon Plate subduction beneath the North American Plate. In the late Miocene, the Comondú rocks were cut by regional NW-SE normal faults with a right lateral movement (e.g., Campamento and Mezquital faults) and NNE-SSW antithetic normal faults with a left lateral movement (e.g., Cimarrón Fault). These faults work under a transtensional tectonic regime associated with the Gulf of California opening. At the same time, the volcanic sequences were interbedded and partially covered by calcareous sediments and sandstones intercalating with siltstones, due to the marine transgression originated by blocks drop and rise. These sediments are unconformably underlain by the Comondú volcanic arc, cropping out to the north of the TVVC in the Azufre Canyon. South of the study area, after a period of 14 Ma, various fissure eruptions occurred and formed an extended basaltic plateau named Esperanza basalt, which covers a large part of the Santa Lucia pyroclastic sequence. North of the TVVC there are sediments overlain by lava flows with peperitic facies, possibly contemporaneous with these

fissure eruptions. After a large erosive and tectonically active period, the volcanic activity was resumed at the northern edge of the study area in the middle Pleistocene. This volcanic activity was highly explosive induced by the Aguajito caldera collapse ~1.17 Ma ago, producing a thick ignimbritic sequence that extended all over the north-northwestern sector.

Subsequently, the TVVC was emplaced along the southern trace of the ~13 km long Cimarron Fault System. To the north, this fault transects the Aguajito caldera (ca. 1.17 Ma) as attested by the stepped morphology and westward rotation of the faults (Figs. 2 and 8). To the south, the Cimarron Fault appears as a series of eruptive fissures along where the complex was emplaced. The TVVC built through the successive construction of El Viejo, El Azufre, and La Virgen volcanoes separated by periods of erosion with the deposition of volcaniclastic, and alluvial fans (df and Al units in figure 2 and 3) at the foot of the volcanoes. These erosive intervals may indicate periods of erosion or volcanic quiescence. The TVC emplaced as a series of eruptive epochs that are summarized below:

***Eruptive Epoch 1: El Viejo Cone (Upper Pleistocene – 300 ka)***

The stratigraphic succession indicates that volcanism in the region was already present at the Reforma and the Aguajito calderas. In the study area, inception of volcanism began during late Pleistocene along the Cimarron Fault. High viscosity lavas erupted to the southwest of the Aguajito Volcanic Complex and formed the Lower Viejo dacitic lava dome. Afterwards, a new effusive eruption produced the Puerta dacitic lava dome (enclave-rich), which flowed over the pre-existing surface of the Aguajito ignimbrite. At around 254 ka, highly viscous lava (enclave-rich) erupted from a fissure extending up to 4 km to the southwest along the middle portion of the Cimarron Fault. This volcanic event (Upper Viejo dacitic lava dome) constructed the entire El Viejo volcano. The enclave-rich dacitic lavas may indicate that magma was opening spaces and tearing the conduit walls en route to the surface. Between 254 and 173 ka, the El Viejo activity

ended and was followed by erosion of the volcano flanks producing lahars and a flank failure of the northern part of the edifice. The collapse generated a debris avalanche some 245 ka towards the North and obstructed the Azufre canyon. This debris avalanche deposit was triggered by weakness of the intense hydrothermally altered rocks of El Viejo.

***Eruptive Epoch 2: El Azufre Stratocone (173–128 ka)***

After a repose period of a few hundred or thousand years, the volcanic activity recommenced about 1 km to the southwest. It centered at the current location of the El Azufre stratocone (ca. 173 ka) discordantly on top of El Viejo cone. The activity began with the eruption of dacitic lava domes on a sloping surface and associated pyroclastic density currents (PDCs) due to the gravitational failure of the external parts of the dome. These PDCs emplaced the Azufre block-and-ash flow deposits which outcrop in the northwestern and southeastern parts of the current El Azufre volcano. After this eruption erosion may have taken place producing volcanoclastic deposits. The volcano remained relatively calm for about 45 ka when a dacitic summit dome was emplaced. After this event, the volcano ceased its activity beginning a period of erosion that dissected the flanks of the cone and generated extended alluvial fans at the base of the volcano.

***Eruptive Epoch 3: Virgen Scoria Cones (128–112 ka)***

Sometime after the extrusion of the El Azufre summit dome, a series of Strombolian eruptions occurred on its southern flank forming a lineament of three scoria cones (Figs. 2 and 3). Their elongated shapes suggest that ascending magma followed the Cimarron Fault. Contemporaneous to the cinder cone formation, a basaltic lava flow erupted from a fissure 4.5 km east of El Azufre volcano followed by another Strombolian eruption. Magmatic activity vented then ~9 km to the southwest of the El Azufre stratocone close to Los Pintos and Las Tres Virgenes valleys respectively, where two scoria cones erupted in successive Strombolian-type eruptions. The scoria fall deposits contain rounded granodioritic enclaves indicating that their magmas ascended

through the Cretaceous batholith. No reliable dates for these cinder cones were obtained, however, their erosional features and stratigraphic relationships allowed us to assign them an age of ~120 ka. During this period volcanic activity occurred at isolated vents around the TVVC forming separate volcanic edifices.

***Eruptive Epoch 4: La Virgen Stratovolcano (112–22 ka)***

After a hiatus of at least 16 ka, magmatism along the Cimarron fissure recommenced some 112 ka with an effusive eruption occurred circa 2.3 km southeast of the El Azufre stratocone. This eruption emplaced the Virgen andesitic neck and the Cueva de Gel andesitic lava that flowed 4.3 km to the east over the Aguajito ignimbrite. Afterwards, volcanic activity migrated 3 km to the southwest to begin the construction of La Virgen stratocone. At 110 ka ago another effusive eruption produced the 7 km long Lower Pintos andesitic lavas that mantled the southwestern and western sectors of El Azufre volcano. These lavas are unusual because of their large volume and extension (Thorpe and Brown, 1985). A second effusive eruption (103 ka) occurred on the northwestern upper flank of La Virgen, emplaced the 4.9 km long the Upper Pintos andesitic lava flow that was channeled between the levees of the Lower Pintos andesitic lava. Soon afterwards, the volcanic activity recommenced with mixed effusive and mild explosive eruptions of the Virgen dacitic lava cone (102 ka) that mantled the main structure of the volcano. Shortly after (89 ka) another effusive event sourced on the northern peak of La Virgen volcano emitted the 5.5 km long Lower Virgen andesitic lava towards the northeastern flank, surrounding and partially overlying the Cueva de Gel andesitic lava. Soon afterwards, another effusive eruption vented on the northwestern upper hillside of La Virgen volcano dispersing the Los Pintos dacitic lava. This lava reached 2.7 km from the crater, and was channeled to the south of the Lower Pintos andesitic lava. At this time, the western flank of La Virgen volcano was highly dissected and eroded forming the Los Pintos Blancos gully. After a repose period of ca. 28 ka, a 2-km long coulée lava

dome draped the southwestern hillside of La Virgen volcano followed by the extrusion of a central dome atop La Virgen volcano. Shortly after, the volcanic activity shifted 3 km to the southern lower flanks of La Virgen emplacing the two small Mezquital dacitic lava domes between 46 and 42 ka, followed by the emission of the Virgen dacitic lava domes (41 ka) on the southwest-south-east lower flanks of the volcano. At around 30 ka (Schmitt et al., 2006; 2010) a rhyolitic magma produced the most explosive eruption of the entire complex. The Plinian eruption of La Virgen Tephra blanketed the southwestern flank and the plains of the region (e.g. Bonfil village) (Capra et al., 1998). Finally, at around 22-25 ka an effusion eruption ensued at the top of La Virgen Volcano dispersed the 10 km long Upper Virgen andesitic lava flow. The black surface of these lava flows lacks any cover and is only sparsely vegetated with dispersed trees.

### **Eruptive Rate**

The total erupted volume of the TVVC is  $39 \text{ km}^3$  over an area of  $120 \text{ km}^2$  during the last ca. 300 ka. By assuming that volcanic activity was continuous we calculated an average eruption rate of  $0.13 \text{ km}^3/\text{kyr}$ . This volume was emitted through effusive eruptions (89 %) with dominantly dacitic (62%), and andesitic compositions (38%). The eruptive volume of the individual volcanic edifices yielded estimates of  $4.2 \text{ km}^3$  for the El Viejo,  $3.8 \text{ km}^3$  for El Azufre, and  $31.2 \text{ km}^3$  for La Virgen volcano. Based on these volumes and ages of each volcanic structure their average eruptive rate corresponds to  $0.076 \text{ km}^3/\text{kyr}$  (El Viejo volcano),  $0.084 \text{ km}^3/\text{kyr}$  (El Azufre volcano), and  $0.35 \text{ km}^3/\text{kyr}$  (La Virgen volcano) (Fig. 11A). The average eruptive rate of La Virgen ( $0.35 \text{ km}^3/\text{kyr}$ ) that involved the extrusion of domes and lava flows is three times larger than the average eruptive rate of the entire TVVC ( $0.13 \text{ km}^3/\text{kyr}$  in  $\sim 300$  ka of activity). The plot of cumulative volume of erupted products against time for the same period (Fig. 11A; e.g., Wadge, 1982) shows a steady state rate with a variable eruptive behavior.



The long-term average eruptive rate of the TVVC was compared with other well-dated large (>400 km<sup>2</sup>) volcanic complexes situated in subduction related environments: the Parinacota (0.28 km<sup>3</sup>/kyr), Tatara-San Pedro (0.06 km<sup>3</sup>/kyr), Seguam (0.25 km<sup>3</sup>/kyr), Ceboruco (0.10 km<sup>3</sup>/kyr), Mt. Adams (0.25 km<sup>3</sup>/kyr), Mt. Baker (0.13 km<sup>3</sup>/kyr), Mt. Mazama (0.42 km<sup>3</sup>/kyr), and Puyehue-Cordón Caulle (0.42 km<sup>3</sup>/kyr) (Singer et al., 2008; Jicha and Singer, 2006) (Fig. 11B). The mean eruption rate of the TVVC (0.13 km<sup>3</sup>/kyr) is comparable with Mt. Baker (0.13 km<sup>3</sup>/kyr) and Ceboruco (0.10 km<sup>3</sup>/kyr), located in the Cascade Volcanic Range, USA, and the western portion of the Trans-Mexican Volcanic Belt, respectively. However, the TVVC shows slower eruption rates if compared with Puyehue-Cordón Caulle, Parinacota, Mt. Adams and, Mt. Mazama in the Cascades, and Seguam in the Aleutians. Tatara-San Pedro in Chile (0.06 km<sup>3</sup>/kyr) has much smaller eruptive rates by an order of magnitude than the TVVC. This comparison indicates that the local tectonic setting of the TVVC favored the high production of magmas and their ascent through a relatively thinner crust in the area if compared to Andean volcanoes that rise through a thick continental crust.

## CONCLUSIONS

The revised geological map and refined stratigraphy of the TVVC aided by new <sup>230</sup>Th/<sup>238</sup>U-zircons and one <sup>206</sup>Pb/<sup>238</sup>U-zircon ages allowed to reconstruct the evolution of the complex. Fault kinematics combined with the distribution of volcanic units and stratigraphy indicate that the location of the TVVC vents were controlled by the NE-SW dextral strike-slip Cimarron Fault. The loci of volcanic vents progressively migrated southwestwards (from El Viejo to La Virgen). The TVVC was built above a basement formed by the Peninsular Ranges Batholith and a superficial basement constituted by the Miocene Santa Lucia pyroclastic flows (21.6 Ma), the Esperanza plateau lavas (7.6 Ma), and Aguajito ignimbrite and pyroclastic deposits (1.1-0.5 Ma).

The chronology of the TVVC occur through four main eruptive epochs during Late Pleistocene with at least sixteen lava units and domes of andesitic to dacitic compositions. The TVVC has experienced at least two explosive eruptions, one ca. 173 ka ago (Azufre dacitic block-and-ash flows) and the ~30 ka Plinian eruption of La Virgen Tephra, a prominent stratigraphic marker in the region. The eruption rates suggest long-term fluctuations in the TVVC with an increase in the eruptive recurrence during the last 112 ka interrupted by relatively large volume eruptions related to the construction of La Virgen volcano. Today, the TVVC is quiescent; however, future activity should not be discarded because it is located in a seismo-tectonic active rift zone with the occurrence of modern earthquakes. These seismic swarms together with aeromagnetic data reveals the presence of dyke swarms possibly related to shallow magmatic sources that feed the Tres Vírgenes geothermal field under exploitation by the Comisión Federal de Electricidad.

#### **ACKNOWLEDGMENTS**

We appreciate the facilities given by the Comisión Federal de Electricidad at the GPG Morelia and Santa Rosalia, and for the use of information of the unpublished internal report DEX-DGL-TV-17. We thank F. Mendiola and F. García for their technical support during the laboratory analyses and D.E. Torres Gaytan for his support during aeromagnetic map generation. This study was partially funded by the Centro Mexicano de Inovación en Energía Geotérmica (CeMIE Geo) projects P15 to J.L. Macías and P17 to V.H. Garduño. We appreciate the discussions held with G. Groppelli and R. Sulpizio during the edition of the map. We appreciate the review of R. Molina to the first draft of this manuscript. We thank A. Schmidt, M.G. Gómez-Vasconcelos, R. Sulpizio and L. Capra for their valuable reviews.

#### **REFERENCES LISTED**

- Avellán, D.R., Macías, J.L., Arce, J.L., Saucedo-Girón, R., Garduño-Monroy, V.H., Jiménez-Haro, A., Sosa-Ceballos G., Cisneros, G., Bernal, J.P., Layer, P.W., Navarrete, J.A., García-Sánchez, L., Reyes-Agustín, G., Rocha, V.S., Rangel, E., López-Loera, H., 2018. Geology of the late Pleistocene Tres Vírgenes Volcanic Complex, Baja California Sur (México). *J. Maps, Manuscript under review*.
- Aguillón-Robles, A., Calmus, T., Benoit, M., Bellon, H., Maury, R., Cotten, J., Bourgois, J., Michaud, F., 2001. Late Miocene adakites and Nb-enriched basalts from Vizcaino Peninsula, Mexico: Indicators of East Pacific Rise subduction below southern Baja California. *Geology* 29(6), 531-534.
- Angelier, J., Colleta, B., Chorowicz, J., Ortlieb, L., Rangin, C., 1981. Faults tectonics of the Baja California peninsula and the opening of the Sea of Cortez, Mexico. *J. Structural Geology* 3, 347-357.
- Antayhua-Vera, Y., Lermo-Samaniego, J., Quintanar-Robles, L., Campos-Enríquez, O., 2015. Seismic activity and stress tensor inversion at Las Tres Vírgenes volcanic and geothermal field (México). *J. Volcanol. Geoth. Res.* 305, 19-29.
- Atwater, T., 1989. Plate tectonic history of the northeast Pacific and western North America, in Winterer, E.L., Hussong, D.M., Decker, R.W., eds., *The eastern Pacific Ocean and Hawaii*: Boulder, Colorado. *Geol. Soc. Am., Geology N. Am. N.*, 21-72.
- Audi, G., Bersillon, O., Blachot, J., Wapstra, A.H., 1997. The NUBASE evaluation of nuclear and decay properties. *Nucl. Physics A.* 624, 1-124.
- Bacon, C.R., Gardner, J.V., Mayer, L.A., Buktenica, M.W., Dartnell, P., Ramsey, D.W., and Robinson, J.E., 2002. Morphology, volcanism, and mass wasting in Crater Lake, Oregon. *Geol. Soc. Am. Bull.* 114, 675–692, doi: 10.1130/0016-7606(2002)114<0675: MVAMWI>2.0.CO;2.
- Bacon, C.R., and Lanphere, M.A., 2006. Eruptive history and geochronology of Mount Mazama and the Crater Lake region, Oregon. *Geol. Soc. Am. Bull.* 118, 1331–1359, doi: 10.1130/B25906.1.
- Batiza, R., 1978. Geology, petrology, and geochemistry of Isla Tortuga, a recently formed tholeiitic island in the Gulf of California. *Geol. Soc. Am. Bull.* 89(9), 1309-1324.
- Bellon, H., Aguillón-Robles, A., Calmus, T., Maury, R.C., Bourgois, J., Cotton, J., 2006. La Purísima volcanic field, Baja California Sur (Mexico): Miocene to Quaternary volcanism related to subduction and opening of an asthenospheric window. *J. Volcanol. Geoth. Res.* 152, 253-272.
- Benoit, M., Aguillón-Robles, A., Calmus, T., Maury, R.C., Bellon, H., Cotton, J., Bourgois, J., Michaud, F., 2002. Geochemical Diversity of Late Miocene Volcanism in Southern Baja California, Mexico: Implication of Mantle and Crustal Sources during the Opening of an Asthenospheric Window. *J. Geol.* 110, 27-648.
- Bernal, J.P., Solari, L.A., Gómez-Tuena, A., Ortega-Obregón, C., Mori, L., Vega-González, M., Espinosa-Arbeláez, D.G., 2014. *In-situ* <sup>230</sup>Th/U dating of Quaternary zircons using LA-MCICPMS. *Quat. Geochronol.* 23, 46-55.

- Boehnke, P., Barboni, M., Bell, E.A., 2016. Zircon U/Th model ages in the presence of melt heterogeneity. *Quat. Geochronol.* 34, 69-74.
- Calmus, T., Aguillón-Robles, A., Maury, R.C., Bellon, H., Benoit, M., Cotton, J., Bourgois, J., Michaud, F., 2003. Spatial and temporal evolution of basalts and magnesian andesites (bajaites) from Baja California, Mexico: the role of slab melts. *Lithos* 66, 77-105.
- Calmus, T., Pallares, C., Maury, R.C., Aguillón-Robles, A., Bellon, H., Benoit, M., Michaud, F., 2011. Volcanic Markers of the Post-subduction Evolution of Baja California and Sonora, Mexico: Slab Tearing Versus Lithospheric Rupture of the Gulf of California. *Pure Appl. Geophys.* 168, 1303-1330.
- Calmus, T., Pallares, C., Maury, R.C., Bellon, H., Pérez-Segura, E., Aguillón-Robles, A., Carreno, A.L., Bourgois, J., Cotten, J., Benoit, M., 2008. Petrologic diversity of Plio-Quaternary post-subduction volcanism in Baja California: an example from Isla San Esteban (Gulf of California, México). *Bull. Soc. Geol. France* 179, 465-481.
- Cameron, K.L., Cameron, M., 1985. Rare earth element,  $^{87}\text{Sr}/^{86}\text{Sr}$ , and  $^{143}\text{Nd}/^{144}\text{Nd}$  compositions of Cenozoic orogenic dacites from Baja California, northwestern Mexico, and adjacent west Texas: evidence for the predominance of a subcrustal component. *Contrib. Mineral. Petrol.* 9, 1-11.
- Campos-Enríquez, J.O. 1992. Geophysical prospecting for geothermal resources in Mexico. *Geofis. Int.* 31(4), 339-340.
- Capra, L., Macías, J.L., Espíndola, J.M., Siebe, C., 1998. Holocene plinian eruption of La Virgen volcano, Baja California, Mexico. *J. Volcanol. Geoth. Res.* 80, 239-266.
- Capra, L., Siebe, C., Macías, J.L., Espíndola, J.M., 2007. Comment on: Schmitt, A.K., et al. (2006): Eruption and magma crystallization ages of Las Tres Vírgenes (Baja California) constrained by combined  $^{230}\text{Th}/^{238}\text{U}$  and (U-Th)/He dating of zircon: Comment: *Journal of Volcanology and Geothermal Research*, v. 163, p. 98-101.
- Cheng, H., Lawrence Edwards, R., Shen, C.C., Polyak, V.J., Asmerom, Y., Woodhead, J., Hellstrom, J., Wang, Y., Kong, X., Spötl, C., Wang, X., Calvin Alexander Jr, E., 2013. Improvements in  $^{230}\text{Th}$  dating,  $^{230}\text{Th}$  and  $^{234}\text{U}$  half-life values, and U-Th isotopic measurements by multi-collector inductively coupled plasma mass spectrometry. *Earth Planet. Sci. Lett.* 371-372, 82-91.
- Conly, A.G., Brennan, J.M., Bellon, H., Scott, S.D., 2005. Arc to rift transitional volcanism in the Santa Rosalía Region, Baja California Sur, Mexico. *J. Volcanol. Geoth. Res.* 142, 303-341.
- Davis, G.H., Reynolds, S.J., Kluth, C.F., 2012. *Structural geology of rocks and regions*: New York, John Wiley and Sons, 839 p.
- Demant, A., 1981. Plio-Quaternary volcanism of the Santa Rosalia area, Baja California, Mexico. In: Ortlieb, L., Roldan, J. (Eds), *Geology of Northwestern Mexico and Southern Mexico and Southern Arizona. Field guides and papers*, pp. 295-307.
- Demant, A., 1984. The Reforma caldera, Santa Rosalia area, Baja California. A volcanical, petrographical and mineralogical study: In Malpica-Cruz, V., Celis-Gutierrez, S., Guerrero-

- García, J., Ortilieb, L. (Eds), Neotectonics and sea level variations in the Gulf of California area. Symposium (Hermosillo, Son. April), pp. 21-23.
- Demant, A., Ortilieb, L., 1981. Plio-Pleistocene volcano-tectonic evolution of la Reforma caldera, Baja California, Mexico. *Tectonophysics*, 71, 194.
- Duque-Trujillo, J., Ferrari, L., Orozco-Esquivel, T., López-Martínez, M., Lonsdale, P., Bryan, S.E., Kluesner, J., Piñero-Lajas, D., Solari, L., 2015. Timing of rifting in the southern Gulf of California and its conjugate margins: insights from the plutonic record. *Geol. Soc. Amer. Bull.* 127, 702–736.
- Ellis, R.G., de Wet, B., MacLeod, I.N., 2012. Inversion of magnetic data for remanent and induced sources. *ASEG Extend Abstracts 2012*, 1-4.
- Fisher, R.V., Schmincke, H.-U., 1984. *Pyroclastic Rocks*. Springer Verlag, Berlin, Heidelberg, pp. 472.
- Garduño-Monroy, V.H., Vargas-Ledezma, H., Campos-Enriquez, J.O., 1993. Preliminary geologic studies of Sierra El Aguajito (Baja California, Mexico): resurgent-type caldera. *J. Volcanol. Geoth. Res.* 59, 47-58.
- García-Sánchez, L., Macías, J.L., Osorio-Ocampo, Sosa-Ceballos, G., Pola, A., Avellán, D.R., Arce, J.L., Saucedo, R., García, F., Reyes-Agustín, G., Cardona, S., Cisneros, G. 2016. Volcanic and magmatic evolution of Reforma Caldera, BCS, Mexico. [Poster], Conf. Cities on Volcanoes 9, September 2016, Puerto Varas, Chile.
- Gastil, R.G., Phillips, R.P., Allison, E.C., 1975. Reconnaissance geology of the state of Baja California. *Mem. Geol. Soc. Am.* 140, 170.
- Germa, A., Connor, L.J., Cañon-Tapia, E., Le Corvec, N., 2013. Tectonic and magmatic controls on the location of post-subduction monogenetic volcanoes in Baja California, Mexico, revealed through spatial analysis of eruptive vents. *Bull. Volcanol.* 75, 1-14.
- Gill, J.B., 1981. *Orogenic Andesites and Plate Tectonics*. Springer, Berlin, 1-390 p.
- Hausback, B.P., 1984. Cenozoic volcanic and tectonic evolution of Baja California Sur, Mexico, in Frizzell, V.A., ed., *Geology of the Baja California Peninsula: Pacific Section*. Soc. Econ. Paleontologists and Mineralogists, 39, 219-236.
- Hausback, B.P., 1992. Blocky pyroclastic flow deposit at Volcano Las Tres Vírgenes, Baja California Sur, Mexico. Tercera Reunión Nacional, Volcán de Colima (abstract). Universidad de Colima, México, 64-65.
- Hausback, B., Abrams, M.J., 1996. Plinian eruption of La Virgen Tephra, Volcan Las Tres Vírgenes, Baja California Sur, Mexico. *Eos. Trans. AGU*, 77 (46 suppl.), 813-814.
- Hausback, B.P., Sawlan, M.G., 1995. Eruption of La Virgen tephra, Volcán Las Tres Vírgenes. Baja California Sur, México. Tercera Reunión Internacional sobre Geología de la Península de Baja California, April, 17-21.
- Heim, A., 1922. Notes on the Tertiary of southern lower California. *Geol. Magazine* 9, 529-547.

- Henderson, R.G., Zietz, I., 1949. The computation of second vertical derivatives of geomagnetic fields. *Geophysics* 14, 508-516.
- Henderson, R.G., 1970. On the validity of the use of upward continuation integral for total magnetic intensity data. *Geophysics* 35, 916-919.
- Hildreth, W., and Lanphere, M.A., 1994. Potassium-argon geochronology of a basalt-andesite-dacite arc system—The Mount Adams Volcanic Field, Cascade Range of Southern Washington. *Geol. Soc. Am. Bull.* 106, 1413–1429, doi: 10.1130/0016-7606(1994)106<1413: PAGOAB>2.3.CO; 2.
- Hildreth, W., Fierstein, J., and Lanphere, M.A., 2003. Eruptive history and geochronology of the Mount Baker volcanic field, Washington. *Geol. Soc. Am. Bull.* 115, 729–764, doi: 10.1130/0016-7606(2003)115<0729: EHAGOT>2.0.CO; 2.
- Hora, J.M., Singer, B.S., and Wörner, G., 2007. Volcano evolution and eruptive flux on the thick crust of the Andean Central Volcanic Zone:  $^{40}\text{Ar}/^{39}\text{Ar}$  constraints from Volcán Parí, Chile. *Geol. Soc. Am. Bull.* 119, 343–362, doi: 10.1130/B25954.1.
- Instituto Nacional de Estadística y Geografía, 2014. Anuario estadístico y geográfico de Baja California Sur. INEGI, México, p. 389.
- Kimbrough, D.L., Smith, D.P., Mahoney, J.B., Moore, T.E., Gastil, R.G., Ortega-Rivera, A., Fanning, C.M., 2001. Forearc basin sedimentary response to rapid Late Cretaceous batholith emplacement in the Peninsular Ranges of southern and Baja California. *Geology* 29, 491-494, doi: 10.1130/0091-7613(2001)029<0491: FBSRTR>2.0.CO; 2.
- Kimbrough, D.L., Abbott, P., Balch, D.C., Hoskin-Bartling, S., Grove, M., Mahoney, J.B., Donohue, R., 2014. Upper Jurassic Peñasquitos Formation - Western wall-rock of the Peninsular Ranges batholith, in Morton, D.M., and Miller, F.K., eds., *Peninsular Ranges Batholith, Baja California and Southern California*. *Geol. Soc. Memoir* 211, 625-643.
- Jaffey, A.H., Flynn, K.F., Glendenin, L.E., Bentley, W.C., M., E.A., 1971. Precision measurement of half-lives and specific activities of  $^{235}\text{U}$  and  $^{238}\text{U}$ . *Phys. Rev. C* 4, 1889-1906.
- Jicha, B.R., and Singer, B.S., 2006. Volcanic history and magmatic evolution of Seguam Island, Aleutian Island arc, Alaska. *Geol. Soc. Am. Bull.* 118, 805–822, doi: 10.1130/B25861.1.
- LeBas, M., Le Maitre, R., Streckeisen, A., Zanettin, B., 1986. A chemical classification of volcanic rocks based on the total alkali-silica diagram. *J. Petrol.* 27, 745-750.
- Lermo, J., Vargas, A., Urban, E., Rodríguez, H., Núñez, F., Espatía, G., 2010. Estudio de sismica pasiva en Las Tres Vírgenes, BCS, Periodo 2010, Instituto de Ingeniería, UNAM [Proyecto CFE-DEV-DGF-TV-25-10]. Gerencia de Proyectos Geotermoeléctricos, Departamento de Exploración, Comisión Federal de Electricidad, México.
- Lonsdale, P., 1989. Geology and tectonic history of the Gulf of California, in Winterer, E.L., Hussong, D.M., Decker, R.W. (Eds), *The Eastern Pacific Ocean and Hawaii*. Boulder, Colorado, *Geol. Soc. Am., Geol. N. Am. N.*, pp. 499-521.

- Le Maitre, R.W., Bateman, P., Dudek, A., Kelller, J., Lameyre Le Bas, M.J., Sabine P.A., Schmid R., Sorensen, H., Streckeisen A., Wolley, A.R., Zanettin, b., 1989. A Classification of igneous rocks and glossary of terms. Blackwell, Oxford, 193 p.
- Lonsdale, P., 1991. Structural patterns of the Pacific floor offshore of Peninsular California, The Gulf and Peninsular Provinces of the Californias: In Dauphin, J.P., Simoneit, B.R.T. (Eds.), Amer. Assoc. Petrol. Geol. Memoir 47, pp. 87-125.
- Ludwig, K.R., 2012. User's manual for Isoplot 3.75: A geochronological Toolkit for Microsoft Excel. Berkeley Geochronology Center, Spec. Pub. 5, 75 p.
- Luhr, J.F., Aranda-Gómez, J.J., Housh, T.B., 1995. San Quintín Volcanic Field, Baja California Norte, México: Geology, petrology, and geochemistry. *J. Geophys. Res.* 100(B7), 10353-10380.
- Macías, J.L., Arce, J.L., Garduño, V.H., Avellán, D.R., García, L., Reyes, G., Rangel, E., Saucedo, R., Cisneros, G., Navarrete, J.A., 2012. Estudio de estratigrafía y geología del Complejo Volcánico Tres Vírgenes, B.C.S. [Informe Final DEX-DGL-TV-17-11]. Comisión Federal de Electricidad, 104 p.
- Macías, J.L. and Jiménez-Salgado, E., 2013. Estudio de Estratigrafía y Geología del Complejo Volcánico Tres Vírgenes, B.C.S. *Geotermia* 26, 14-23.
- Marti, J., Gropelli, G., Silveira, A. 2018. Volcanic stratigraphy: A review. *J. Volcanol. Geoth. Res.* 357, 68-91.
- Martín, A., Fletcher, J.M., López-Martínez, M., Mendoza-Borunda, R., 2000. Waning Miocene subduction and arc volcanism in Baja California: the San Luis Gonzaga volcanic field. *Tectonophysics*, 318, 27-51.
- Müller, W., Shelley, M., Miller, P., Broude, S., 2009. Initial performance metrics of a new custom-designed ArF excimer LA-ICP-MS system coupled to a two-volume laser-ablation cell. *J. Analytical Atomic Spectrom.* 24, 209-214.
- Negrete-Aranda, R., Cañon-Tapia, E., 2008. Post-subduction volcanism in the Baja California Peninsula, Mexico: The effects of tectonics reconfiguration in volcanic systems. *Lithos* 102, 392-414.
- Osorio-Ocampo, S., Macías, J.L., García-Sánchez, Sosa-Ceballos, G., Pola, A., García-Tenorio, F., 2016. Calc-alkaline magmatism of El Aguajito Caldera, Baja California Sur, México. [Poster], Conf. Cities on Volcanoes 9, September 2016, Puerto Varas, Chile.
- Pallares, C., Maury, R.C., Bellon, H., Royer, J.Y., Calmus, T., Aguillón-Robles, A., Cotton, J., Benoit, M., Michaud, F., Bourgois, J., 2007. Slab-tearing following ridge-trench collision: Evidence from Miocene volcanism in Baja California, Mexico. *J. Volcanol. Geoth. Res.* 161, 95-117.
- Pallares, C., Bellon, H., Benoit, M., Maury R.C., Aguillón-Robles, A., Calmus, T., Cotten, J., 2008. Temporal geochemistry evolution of Neogene volcanism in northern Baja California (27°-30° N): Insights on the origin of post-subduction magnesian andesites. *Lithos*, 105, 162-180.

- Paton, C., Hellstrom, J., Paul, B., Woodhead, J., Hergt, J., 2011. Iolite: Freeware for the visualisation and processing of mass spectrometric data. *J. Analytical Atomic Spectrom.* 26, 2508-2518.
- Paton, C., Woodhead, J.D., Hellstrom, J.C., Hergt, J.M., Greig, A., Maas, R., 2010. Improved laser ablation U-Pb zircon geochronology through robust downhole fractionation correction. *G<sup>3</sup>, Geochemistry, Geophysics, Geosystems. An Electronic J. Earth Sci.* 11, 1-36.
- Soto-Peredo, J., Lorenzo-Pulido, C. 2012. Sismicidad en el complejo volcánico de Las Tres Vírgenes, B. C. S. *Geotermia* 26(1), 34-43.
- Petrus, J.A., Kamber, B.S., 2012. VizualAge: A Novel Approach to Laser Ablation ICP-MS U-Pb Geochronology Data Reduction. *Geostand. Geoanal. Res.* 36(3), 247-270.
- Romo, J.M., Wong, V., Flores, C., Vázquez, R., 2000. The subsurface electrical conductivity and the attenuation of coda waves al Las Tres Vírgenes geo-thermal field in Baja California Sur, México. *Proceedings of the 2000 Worl Geotherm. Congress, Int. Geotherm. Assoc.* 1645-1650.
- Ryan, W.B.F., Carbotte, S.M., Coplan, J.O., O'hara, S., Melkonian, A., Arko, R., Weissel, R.A., Ferrini, V., Goodwillie, A., Nitsche, F., Bonczkowski, J., Zemsky, R., 2009. Global Multi-Resolution Topography synthesis. *Geochem. Geophys. Geosyst.* 10, 1-9.
- Saunders, A.D., Rogers, G., Marriner, G.F., Terrell, D.J., Verma, S.P., 1987. Geochemistry of Cenozoic volcanic rocks, Baja California, Mexico: implications for the petrogenesis of post-subduction magmas. *J. Volcanol. Geother. Res.* 32, 223-245.
- Sawlan, M.G., Smith J.G., 1984. Petrologic characteristics, age and tectonic setting of Neogene volcanic rocks in northern Baja California Sur, Mexico. In: Frizzel, V.A. (Ed.), *Geology of the Baja California Peninsula, Pacific Section. Soc. Econ. Paleontologists and Mineralogists*, 237-251.
- Sawlan, M.G., 1986. Petrogenesis of Late Cenozoic volcanic rocks from Baja Califronia Sur, Mexico [Ph.D. thesis]. Santa Cruz, University of California, 174 p.
- Sawlan, M.G., 1991. Magmatic evolution of the Gulf of California rift. In: Dauphin, J.P., Simoneit, B.R.T. (Eds.), *The Gulf and Peninsular Province of the Californias. Am. Assoc. Petr. Geol. Mem.* 47, 301-369.
- Schmidt, E.K., 1975. Plate tectonics, volcanic petrology, and ore formation in the Santa Rosalia area, Baja California, Mexico [Master's thesis]. Tucson, University of Arizona, 194 p.
- Schmitt, A.K., Stockli, D.F., Hausback, B.P., 2006. Eruption and magma crystallization ages of Las Tres Vírgenes (Baja California) constrained by combined  $^{230}\text{Th}/^{238}\text{U}$  and (U-Th)/He dating of zircon. *J. Volcanol. Geother. Res.* 158, 281-295.
- Schmitt, A.K., Stockli, D.F., Niedermann, S., Lovera, O.M., Hausback, B.P., 2010. Eruption ages of Las Tres Vírgenes (Baja California). A tale of two helium isotopes. *Quat. Geochronol.* 5, 503-511.



- Silver, L.T., Chappell, B., 1988. The Peninsular Ranges batholith: An insight into the Cordilleran batholiths of southwestern North America: *Transections of the Royal Society of Edinburg. Earth Sci.* 79, 105-121, doi: 10.1017/S0263593300014152.
- Singer, B.S., Thompson, R.A., Dungan, M.A., Feeley, T.C., Nelson, S.T., Pickens, J.C., Brown, L.L., Wulff, A.W., Davidson, J.P., and Metzger, J., 1997. Volcanism and erosion during the past 930 ky at the Tatara-San Pedro complex, Chilean Andes. *Geol. Soc. Am. Bull.* 109, 127–142, doi: 10.1130/0016-7606(1997)109<0127: VAEDTP>2.3.CO; 2.
- Singer, B.S., Jicha, B.R., Harper, M. A., Naranjo, J.A., Lara L.E., Moreno-Roa, H., 2008. Eruptive history, geochronology, and magmatic evolution of the Puyehue-Cordón Caulle volcanic complex, Chile. *Geol. Soc. Am. Bull.* 120(5/6), 599-618; doi: 10.1130/B26276.1
- Sláma, J., Kosler, J., Condon, D.J., Crowley, J.L., Gerdes, A., Hanchar, J.M., Horstwood, M.S.A., Morris, G.A., Nasdala, L., Norberg, N., Schaltegger, U., Schoene, B., Tubrett, M.N., Whitehouse, M.J., 2008. Plesovice zircon –A new natural reference material for U-Pb and Hf isotopic microanalysis. *Chem. Geology*, 149(1-2), 1-35.
- Solari, L.A., Gómez-Tuena, A., Bernal, J.P., Pérez-Arvizu, O., Tanner, M., 2010. U-Pb zircon geochronology by an integrated LA-ICPMS microanalytical workstation: achievements in precision and accuracy. *Geostand. Geoanal. Res.* 34(1), 5-18.
- Spector, A., Grant, S., 1970. Statistical models for interpreting aeromagnetic data. *Geophysics*, 35, 293-302.
- Stock, J.M., Hodges, K.V., 1989. Pre-Pliocene extension around the Gulf of California and the transfer of Baja California to the Pacific Plate. *Tectonics* 8(1), 99-115.
- Stock, J.M., Lee, J., 1994. Do microplates in subduction zones leave a geological record? *Tectonics* 13(6), 1472-1487.
- Sun S.S., McDonough W.F., 1989. Chemical and isotopic systematics of oceanic basalts-implications for mantle composition and process. In: Sanunders A.D., Norry M.J. (Eds.) *Magmatism in the ocean basins*. *Geol. Soc. Lon. Spec. Publ.* 42, 313-345.
- Thorpe R.S., Brown G.C., 1985. The field description of igneous rocks. *Geol. Soc. London Handbook Series*, 154 p.
- Umhoefer, P.J., Dorsey R.J., Willsey S., Mayer L., Renne P., 2001. Stratigraphy and geochronology of the Comondú group near Loreto, Baja California sur, Mexico. *Sediment. Geol.* 144, 125-147.
- Vidal-Solano, J., Paz-Moreno, F.A., Iriondo, A., Demant, A., Cochemé, J.J., 2005. Middle Miocene peralkaline ignimbrites in the Hermosillo region (Sonora, Mexico): Geodynamic implications. *C.R. Geoscience* 337, 1421-1430.
- Wadge, G., 1982. Steady state volcanism: Evidence from eruption histories of polygenetic volcanoes. *J. Geophys. Res.* 87, 4035-4049.

- Wiedenbeck, M., Hanchar, J.M., Peck, W.H., Sylvester, P., Valley, J., Whitehouse, M., Kronz, A., Morishita, Y., Nasdala, L., Fiebig, J., Franchi, I., Girard, J.P., Greenwood, R.C., Hinton, R., Kita, N., Mason, P.R.D., Norman, M., Ogasawara, M., Piccoli, P.M., Rhede, D., Satoh, H., Schulz-Dobrick, B., Skår, O., Spicuzza, M.J., Terada, K., Tindle, A., Togashi, S., Vennemann, T., Xie, Q., Zheng, Y.F., 2004. Further Characterisation of the 91500 Zircon Crystal. *Geostand. Geoanal. Res.* 28, 9-39.
- Wong, V., 2000. Estudio de sismotectónica, atenuación y tomografía sísmica en la region volcánica y geotérmica Las Tres Vírgenes, Baja California Sur, México. [Ph.D. Thesis]. CICESE, Seismology Department, Earth Sciences Division, Ensenada, Baja California, Mexico, p. 182.
- Wong, V., Munguia, L., 2006. Seismicity, focal mechanism, and stress distribution in the Tres Vírgenes volcanic and geothermal region, Baja California Sur, Mexico. *Geofísica Internacional*, 45, 23-37.

**FIGURE CAPTIONS**

**Figure. 1.** Inset. Location of the the TVVC and Baja California Peninsula in Mexico; Regional tectonic regime showing the active synrift process of the Gulf of California, subject to a transtensional stress regime with a domain of right-lateral fault systems. The boundaries of the Pacific and Rivera oceanic plates as well as the Salton Trough and Tosco-Abreojos fault zones are also indicated. The study area is located by the yellow star. Shape relief map and bathymetric data was acquired and modified from Ryan et al. (2009).

**Figure. 2.** A simplified geological map of the area that includes four basement units (Peninsular Ranges Batholith, Santa Lucia Formation, Esperanza Basalt, and Aguajito Caldera), and the youngest TVVC (after Avellán et al., 2018). The TVVC is made of 19 stratigraphic units in accordance with the description of units of Marti et al. (2018) that are shown in the composite column in figure 3. The map shows towns, main roads, and the location of stratigraphic units, sampling sites, faults, and the CFE exploratory wells. Digital Elevation Model (DEM) with a 5-m<sup>2</sup> resolution.

**Figure. 3.** Stratigraphic composite column of the basement rocks (Peninsular Ranges Batholith, Santa Lucia Formation, Esperanza Basalt, and Aguajito Caldera), volcanoclastic formations, and the late Pleistocene succession of the TVVC composed of 19 units (see discussion of volcanic terminology in Marti et al., 2018) displayed in the geological map of figure 2. Eruptive epoch stands for activity that occurs in tens of years to ka according to Fisher and Schmincke (1984).

**Figure 4.** <sup>206</sup>Pb/<sup>238</sup>U age plot for the Santa Lucia Formation. The graph on the left corresponds to the average age and the graph on the right corresponds to the Concordia age line.

**Figure 5.** A-F, Diagrams of zircon modeled ages of selected samples of this study.

**Figure 6.** A) TAS diagram (LeBas et al., 1986) of the TVVC, Santa Lucia Formation, the Peninsular Ranges Batholith and enclave rocks. B) SiO<sub>2</sub> vs. K<sub>2</sub>O diagram, modified from Gill

(1981), using the subdivisions of Le Maitre et al. (1989). C-D) Plot of abundance of trace elements, normalized with primitive mantle values (Sun and McDonough, 1989). Multi-element diagram, normalized with the chondritic values of Sun and McDonough (1989). E) Time (ka) vs. SiO<sub>2</sub> (in wt. %) diagram (ages are based on <sup>230</sup>Th-U zircon and <sup>206</sup>Pb/<sup>238</sup>U zircon geochronology used to build the stratigraphic composite column (Fig. 3).

**Figure 7.** A) Hypsometric model that shows the main morphological characteristics of the area, where NE-SW and NW-SE patterns are clearly observed in the relief. Light colors correspond to low elevations while warm colors correspond to high elevations; B) Panoramic photograph showing the soft escarp of the Reforma Fault and the sediments of Santa Lucia Range on the SW hanging wall; C) Photograph that shows the plain of the Campamento Fault, with a vertical escarpment of 200 meters and its hanging wall falling to the NE; D) Google earth image showing the right strike-slip Bonfil Fault, where it is possible to observe the ca. 400 m right lateral displacement in rivers and volcanic structures.

**Figure 8.** A) Structural map of major faults and large-scale fractures in the area. Focal mechanisms on top from Wong et al. (2006) and Antayhua-Vera et al. (2015). Below appear the statistical and structural analyses of fault and fracture planes data associated with regional faults; blue numbers represent focal mechanism of Wong et al. (2006), and orange numbers structural stations. B) Structural block map showing the tectonic-structural relationship between the TVVC, the regional faults and current stress field, blocks are bounded by faults with best morphological expression

**Figure 9.** Image of the Magnetic Field Reduced to the Pole (MFRP). The MFRP values are represented by horizontal bar color at the base of the figure with red colors representing high values and the blue ones the low value of magnetic intensities. The hourglass symbol represents the CFE wells and triangles represents the volcanoes of TVVC.

**Figure 10.** 3D inversion model of the magnetic susceptibility produced with the Geosoft's VOXI software by using the magnetic vector inversion method (Ellis et al., 2012). In this image two anomalies related to large intrusive bodies (magmatic reservoirs) with shallow swarms of dikes occur at depths between 0.2 to >7 km below the surface. Geological profile of the TVVC summarizing the results of this study, colors of units as those of figure 3.

**Figure 11.** A) Time (ka) versus cumulative volume (km<sup>3</sup>) of the TVVC. B) Comparison with TVVC with other volcanoes; only the past 400 ka of record at each volcano are considered here. Data from: Hildreth and Lanphere (1994), Singer et al. (1997), Bacon et al. (2002), Hildreth et al. (2003), Frey et al. (2004), Bacon and Lanphere (2006), Jicha and Singer (2006), Hora et al. (2007), and Singer et al. (2008).

## TABLES

**Table 1.** <sup>206</sup>Pb/<sup>238</sup>U-zircon age for Santa Lucia Formation.

**Table 2.** List of the <sup>230</sup>Th/<sup>238</sup>U-zircon model-ages of samples analyzed in this study. Zircon model ages indicate magmatic crystallization from a zircon-saturated melt. They are thus a maximum for the eruption age. Where available, (U-Th)/He zircon ages defining the eruption and the youngest <sup>230</sup>Th-U zircon crystallization ages overlap (Schmitt et al., 2010). This suggests that the eruption terminated zircon crystallization at least for some crystals, and that the youngest <sup>230</sup>Th-U zircon crystallization age is a reasonable proxy for the eruption age. This is supported by <sup>40</sup>Ar-<sup>39</sup>Ar dates and the detailed stratigraphy established through mapping.

**Table 3.** Whole-rock chemistry of juvenile and enclave samples of the TVVC discussed in this study.

## APPENDIX 1.

<sup>206</sup>Pb/<sup>238</sup>U and <sup>230</sup>Th/<sup>238</sup>U zircons analysis results for whole-rock samples from TVVC.

Table 1

Sample	Location		Lithostratigraphic unit	$^{206}\text{Pb}/^{238}\text{U}$ Age [Ma]	+	-
	North	West				
Rf20	3032372	346609	SL	21.59	0.29	0.29

ACCEPTED MANUSCRIPT

Table 2

Sample	Location		Lithostratigraphic unit	$^{230}\text{Th}$ age model [ka]	+	-
	North	West				
TV1101	3043318	345067	Abaf	146,495	27,887	22,188
TV1104	3043234	344350	Adcd	153,939	32,548	25,034
TV1161	3040774	348821	CGal	112,389	26,039	21,004
TV1153	3044164	339413	UPal	103,781	12,400	11,133
TV1121	3037089	341814	Pdcd	61,207	7,162	6,720
TV1147	3039266	342826	Vdcd	51,343	8,754	8,103
TV1118	3036740	342519	Vdid	41,223	6,088	5,766

ACCEPTED MANUSCRIPT

Table 3 continued

Sample	LV2	LV2	TV1152	TV1156	TV1157	TV1159	TV1101	TV1102	TV1104	TV1179	TV1178B	TV1178A	TV1177	TV1176	
Location	North	3046304	3046304	3044533	3046856	3047579	3046791	3043318	3043270	3043234	3042184	3042533	3042533	3042798	3042839
	East	345540	345540	337738	340423	341912	345158	345067	344483	344350	343590	343556	343556	343482	343359
Unit		PRB	PRB	SF	SF	SF	LVdld	Abaf	Abaf, enclave	Adcd	Vsc	Vsc, enclave	Vsc	Vsc	Vsc
Age		99.1 +/-0.8 Ma	99.1 +/-0.4 Ma	11 - 25 Ma	11 - 25 Ma	11 - 25 Ma	ca. 300 ka	173 ka	-	128 ka	-	-	-	-	-
Major Elements (wt. %)															
SiO <sub>2</sub>	57.57	61.12	72.03	61.81	57.72	64.42	64.94	58.52	64.76	51.26	49.91	51.16	51.33	51.04	
Al <sub>2</sub> O <sub>3</sub>	16.8	15.86	13.35	15.61	18.2	16.06	15.17	16.59	15.13	16.96	25.14	16.69	16.73	16.46	
Fe <sub>2</sub> O <sub>3</sub>	6.36	5.7	1.57	5.17	5.69	4.4	5	6.93	4.71	8.53	3.56	8.55	8.66	8.64	
MnO	0.109	0.068	0.047	0.075	0.095	0.076	0.086	0.115	0.08	0.129	0.06	0.128	0.13	0.13	
MgO	2.58	2.71	0.39	2.59	3.96	1.85	1.95	3.37	1.77	6.18	4.77	6.15	6.28	6.37	
CaO	6.07	4.59	1.09	4.74	7.78	4.43	4.52	6.91	4.17	9.67	14.5	9.57	9.7	9.67	
Na <sub>2</sub> O	4.26	4.32	3.56	3.77	4.05	4.33	4.24	4.1	4.31	3.61	2.42	3.68	3.66	3.56	
K <sub>2</sub> O	1.81	2.49	4.66	3.27	0.99	1.83	1.92	0.89	2.03	0.69	0.12	0.73	0.67	0.68	
TiO <sub>2</sub>	1.235	0.891	0.202	0.762	0.77	0.59	0.837	1.119	0.764	1.552	0.277	1.539	1.538	1.51	
P <sub>2</sub> O <sub>5</sub>	0.31	0.2	0.03	0.19	0.17	0.12	0.15	0.2	0.15	0.33	0.06	0.35	0.36	0.34	
LOI	3.05	0.65	3.39	1.08	0.65	0.95	1.69	0.92	1.2	0.22	0.07	0.05	0.34	0.54	
Total	100.1	98.59	100.3	99.06	100.1	99.06	100.5	99.65	99.09	99.13	100.9	98.6	99.39	98.94	
Trace elements (ppm)															
Be	2	2	2	2	< 1	1	1	< 1	1	< 1	< 1	< 1	< 1	< 1	
S	0.052	0.005	0.002	0.006	0.009	< 0.001	0.003	0.057	0.004	0.012	< 0.001	0.006	0.035	0.039	
Sc	16	12	3	12	18	9	12	19	11	24	18	24	24	25	
V	160	111	18	113	149	103	125	181	110	215	70	219	208	215	
Cr	70	30	< 20	50	< 20	20	< 20	< 20	< 20	140	200	150	140	150	
Co	17	12	28	13	35	9	30	35	36	30	18	31	30	31	
Ni	33	28	5	37	6	21	6	6	6	74	44	75	80	81	
Cu	45	8	4	44	20	19	7	15	6	37	31	40	45	45	



Zn	73	50	42	54	63	49	62	71	59	68	17	65	70	75
Ga	20	16	13	16	16	16	16	17	16	18	15	18	17	18
Ge	1	1	1	1	1	1	1	1	1	2	1	2	1	2
As	5	< 5	< 5	< 5	< 5	< 5	< 5	< 5	< 5	< 5	< 5	< 5	< 5	< 5
Se	< 3	< 3	< 3	< 3	< 3	< 3	< 3	< 3	< 3	< 3	< 3	< 3	< 3	< 3
Br	< 0.5	< 0.5	< 0.5	< 0.5	< 0.5	< 0.5	< 0.5	< 0.5	< 0.5	< 0.5	< 0.5	< 0.5	< 0.5	8.4
Rb	37	58	116	98	11	38	42	16	46	6	< 2	5	5	4
Sr	578	561	139	488	762	405	383	502	367	997	407	981	1004	1004
Y	17	10	15	19	12	14	20	20	18	17	5	16	16	17
Zr	260	233	138	240	83	108	138	121	134	108	20	106	110	105
Nb	8	7	8	9	2	4	5	3	5	4	< 1	4	4	4
Mo	6	4	4	5	< 2	4	< 2	< 2	< 2	3	3	3	3	3
Ag	< 0.3	< 0.3	< 0.3	0.5	0.5	0.5	< 0.3	0.3	< 0.3	0.4	< 0.3	0.4	0.5	0.5
Cd	< 0.5	< 0.5	< 0.5	< 0.5	< 0.5	< 0.5	< 0.5	< 0.5	< 0.5	< 0.5	< 0.5	< 0.5	< 0.5	< 0.5
In	< 0.2	< 0.2	< 0.2	< 0.2	< 0.2	< 0.2	< 0.2	< 0.2	< 0.2	< 0.2	< 0.2	< 0.2	< 0.2	< 0.2
Sn	2	2	3	2	< 1	3	2	1	2	1	< 1	1	< 1	1
Sb	1.5	< 0.5	0.8	< 0.5	< 0.5	< 0.5	< 0.5	< 0.5	< 0.5	< 0.5	< 0.5	< 0.5	< 0.5	< 0.5
Cs	2.5	2.7	4.8	4.6	0.6	1.2	1.7	0.7	1.9	< 0.5	< 0.5	< 0.5	< 0.5	< 0.5
Ba	586	680	905	973	470	558	535	318	569	307	63	273	280	275
La	23.5	24	30.1	25.1	9.1	11.9	13.8	9.8	14.6	12.2	2	11.3	11.3	11.2
Ce	52.3	50.9	56.5	53.4	20.3	24.9	29.2	22.6	31.3	29.7	4.9	28.9	28.9	28.6
Pr	6.44	5.87	5.79	6.11	2.5	2.85	3.55	2.98	3.72	4.1	0.71	3.99	4.07	4.03
Nd	26.7	20.9	19	23.3	10.4	11.2	14.6	13	14.5	18.3	3.5	18	17.9	18.3
Sm	5.6	3.4	3.1	4.5	2.3	2.4	3.3	3.2	3.3	4.1	1	4.1	4.2	4.1
Eu	1.43	1.06	0.43	0.92	0.77	0.67	0.87	1.03	0.85	1.39	0.57	1.34	1.36	1.39
Gd	4.7	2.5	2.4	3.7	2.1	2.4	3.3	3.5	3.1	3.9	1.1	3.8	3.9	4
Tb	0.7	0.3	0.4	0.6	0.3	0.4	0.6	0.6	0.5	0.6	0.2	0.6	0.6	0.6
Dy	3.6	1.9	2.3	3.2	2	2.3	3.3	3.4	3.1	3.5	1.1	3.5	3.5	3.5
Ho	0.7	0.4	0.5	0.6	0.4	0.5	0.7	0.7	0.6	0.7	0.2	0.7	0.7	0.7
Er	1.9	1	1.5	1.9	1.2	1.5	2	2	1.9	2	0.7	2	2	2
Tm	0.29	0.15	0.23	0.27	0.17	0.22	0.3	0.31	0.28	0.29	0.1	0.3	0.29	0.3

Yb	1.8	1	1.6	1.7	1.1	1.5	2	2	2	1.9	0.6	1.8	1.8	1.9
Lu	0.27	0.16	0.29	0.28	0.18	0.25	0.32	0.31	0.32	0.27	0.1	0.27	0.27	0.26
Hf	6.1	5.1	3.8	5.5	2	2.7	3.7	2.8	3.3	2.6	0.5	2.6	2.6	2.5
Ta	0.6	0.4	1.2	0.7	0.4	0.4	0.7	0.5	0.7	0.2	<0.1	0.2	0.2	0.2
W	<1	<1	208	<1	186	<1	174	189	241	<1	<1	<1	<1	<1
Ir	<5	<5	<5	<5	<5	<5	<5	<5	<5	<5	<5	<5	<5	<5
Au	<2	<2	<2	<2	10	<2	<2	<2	<2	<2	<2	<2	<2	<2
Tl	0.2	0.2	0.6	0.2	<0.1	0.2	0.2	<0.1	0.2	<0.1	<0.1	<0.1	<0.1	<0.1
Pb	8	<5	15	10	<5	<5	9	<5	<5	<5	<5	<5	<5	<5
Bi	<0.4	<0.4	<0.4	<0.4	<0.4	<0.4	<0.4	<0.4	<0.4	<0.4	<0.4	<0.4	<0.4	<0.4
Th	8.7	8	17.7	14.6	1.1	3.4	3.9	1.7	4.2	0.7	0.3	0.8	0.7	0.7
U	1.7	3.4	5.3	4.3	0.4	1.2	1.4	0.6	1.5	0.2	<0.1	0.2	0.2	0.2
Sr/Y	34.00	56.10	9.27	25.68	63.50	28.93	19.15	25.10	20.39	58.65	81.40	61.31	62.75	59.06
La/Yb	13.06	24.00	18.81	14.76	8.27	7.93	6.90	4.90	7.30	6.42	3.33	6.28	6.28	5.89

Table 3 continued

Sample	TV1160	TV1138	TV1129B	TV1161	TV1129A	TV1149	TV1155	TV1124B	TV1125B	TV1153	TV1123	TV1109	TV1127	TV1128
Location	North 3042198	3037944	3040214	3040774	3040214	3040046	3046402	3041325	3041095	3044164	3041440	3037934	3040681	3040615
	East 348407	340051	340661	348821	340661	343276	339817	339753	339951	339413	339714	344624	340453	340760
Unit	Vsc	Vsc	Vsc, removed	CGal	Van	Van	LPal	LPal	LPal, enclave	UPal	UPal	Vdlc	Pdl	Pdl
Age	-	-	-	112 +26/- 21 ka	ca. 111 ka	ca. 111 ka	110.6 +43/- 30.9 ka	110.6 +43/- 30.9 ka	-	103.8 +12/- 11 ka	103.8 +12/-11 ka	102 +30/- 23.8 ka	89.6 +11.9/- 10.7 ka	89.6 +11.9/- 10.7 ka
Major Elements (wt. %)														
SiO <sub>2</sub>	51.64	55.45	58.54	61.98	62.21	60.15	57.34	63.51	55.77	61.78	61.99	63.8	64.44	65.44
Al <sub>2</sub> O <sub>3</sub>	16.07	17.48	17.44	16.91	16.65	17.15	17.84	16.19	12.13	16.42	15.88	16.06	16.17	15.65
Fe <sub>2</sub> O <sub>3</sub>	10.2	7.33	6.52	5.72	5.5	6.8	6.76	4.72	6.88	5.48	4.95	4.69	4.91	4.76
MnO	0.158	0.111	0.106	0.094	0.092	0.107	0.11	0.081	0.174	0.091	0.085	0.079	0.082	0.081
MgO	6.63	5.39	3.65	2.97	2.15	2.92	3.76	2.39	8.79	2.87	2.48	2.5	2.25	2.01

	CaO	9.93	8.79	7.14	5.95	5.24	6.73	7.68	4.94	10.93	5.94	5.18	5.06	4.96	4.37
	Na <sub>2</sub> O	3.69	3.77	4.3	4.39	4.45	4.27	4.18	4.28	2.78	3.98	4.27	4.25	4.25	4.17
	K <sub>2</sub> O	0.45	0.8	1	1.46	1.34	0.99	1.05	1.84	0.86	1.84	1.97	1.76	1.89	2.18
	TiO <sub>2</sub>	1.646	1.147	1.024	0.824	0.908	0.997	1.014	0.735	0.756	0.798	0.824	0.711	0.722	0.719
	P <sub>2</sub> O <sub>5</sub>	0.24	0.23	0.21	0.18	0.16	0.14	0.22	0.15	0.07	0.19	0.2	0.17	0.17	0.16
	LOI	0.13	0.48	0.35	0.07	1	-0.01	0.68	0.28	1.45	1.06	1.45	0.84	1.1	0.95
	Total	100.8	101	100.3	100.5	99.71	100.2	100.6	99.11	100.6	100.5	99.27	99.91	100.9	100.5
Trace elements (ppm)															
	Be	< 1	< 1	1	1	1	< 1	< 1	1	1	1	1	1	1	1
	S	0.01	0.005	0.002	0.008	0.002	0.002	0.048	0.002	0.011	0.009	0.001	< 0.001	0.005	0.004
	Sc	34	20	18	14	13	16	17	11	59	13	12	11	10	10
	V	267	179	169	126	124	159	157	102	210	121	117	103	102	97
	Cr	100	90	30	30	< 20	40	30	< 20	790	30	< 20	< 20	20	< 20
	Co	32	23	15	14	36	15	17	29	40	13	36	32	10	10
	Ni	55	62	17	22	6	29	16	17	63	21	6	20	20	17
	Cu	39	53	30	28	11	33	19	18	5	29	8	12	16	13
	Zn	67	67	77	62	60	61	66	60	101	63	61	58	56	54
	Ga	17	16	16	17	17	17	18	16	13	17	16	16	16	16
	Ge	2	1	1	1	2	1	1	1	2	1	1	1	1	1
	As	< 5	< 5	< 5	< 5	< 5	< 5	< 5	< 5	< 5	< 5	< 5	< 5	< 5	< 5
	Se	< 3	< 3	< 3	< 3	< 3	< 3	< 3	< 3	< 3	< 3	< 3	< 3	< 3	< 3
	Br	< 0.5	< 0.5	< 0.5	< 0.5	< 0.5	< 0.5	< 0.5	< 0.5	< 0.5	< 0.5	< 0.5	< 0.5	< 0.5	< 0.5
	Rb	< 2	7	16	27	25	17	13	39	12	28	38	37	37	44
	Sr	598	789	605	554	408	448	753	500	251	535	599	516	498	440
	Y	24	15	16	17	21	17	16	16	17	16	17	15	17	18
	Zr	113	84	95	119	146	105	103	122	52	116	141	121	120	139
	Nb	3	4	3	4	5	3	3	4	3	4	5	4	4	5
	Mo	2	5	3	3	< 2	6	4	< 2	< 2	4	< 2	< 2	4	4
	Ag	0.4	< 0.3	< 0.3	0.6	0.5	< 0.3	0.4	< 0.3	< 0.3	0.3	0.5	0.4	0.3	0.4
	Cd	< 0.5	< 0.5	< 0.5	< 0.5	< 0.5	< 0.5	< 0.5	< 0.5	< 0.5	< 0.5	< 0.5	< 0.5	< 0.5	< 0.5

In	<0.2	<0.2	<0.2	<0.2	<0.2	<0.2	<0.2	<0.2	<0.2	<0.2	<0.2	<0.2	<0.2	<0.2
Sn	1	2	17	2	2	2	2	2	2	3	3	2	3	3
Sb	<0.5	<0.5	<0.5	<0.5	<0.5	<0.5	<0.5	<0.5	<0.5	<0.5	<0.5	<0.5	<0.5	<0.5
Cs	<0.5	<0.5	0.8	0.7	1	0.8	0.5	1	1.5	1.1	1.5	1.5	1.5	1.8
Ba	184	332	389	475	420	361	358	510	241	475	533	499	490	544
La	7.4	9.3	10.4	11.9	11.8	8.8	11.1	13.3	10.9	12.2	14.8	13.1	13.2	14.1
Ce	20	23.1	24.2	26.4	27.3	20.6	26.4	28.9	21.7	27.5	33.4	28.5	28.6	30.3
Pr	2.88	3.03	3.03	3.22	3.34	2.66	3.32	3.35	2.67	3.27	3.96	3.4	3.39	3.54
Nd	13.5	13.3	13.2	13.4	14.1	11.8	14.1	13.6	11.5	13.5	15.9	13.5	13.7	14.3
Sm	3.6	2.9	3.1	2.9	3.3	2.9	3.2	3	2.9	3	3.5	3	3	3.1
Eu	1.32	0.97	1	0.85	0.94	0.92	1	0.77	0.84	0.84	0.95	0.79	0.82	0.77
Gd	4	2.7	3	2.9	3.5	3	3	2.9	3.2	2.9	3.2	2.8	2.8	3
Tb	0.7	0.4	0.5	0.5	0.6	0.5	0.5	0.5	0.5	0.5	0.5	0.5	0.5	0.5
Dy	4.2	2.4	2.9	2.8	3.3	3	2.7	2.7	2.9	2.8	3	2.7	2.7	3
Ho	0.9	0.5	0.6	0.6	0.7	0.6	0.6	0.6	0.6	0.6	0.6	0.5	0.6	0.6
Er	2.5	1.4	1.6	1.7	2.1	1.9	1.6	1.7	1.6	1.7	1.8	1.6	1.7	1.8
Tm	0.36	0.2	0.24	0.25	0.3	0.28	0.23	0.26	0.24	0.26	0.26	0.24	0.26	0.27
Yb	2.4	1.3	1.6	1.7	2	1.8	1.5	1.7	1.6	1.7	1.8	1.7	1.7	1.8
Lu	0.37	0.21	0.26	0.27	0.33	0.29	0.25	0.28	0.25	0.27	0.3	0.26	0.29	0.31
Hf	2.6	2	2.4	2.8	3.3	2.7	2.5	3	1.6	2.9	3.3	3.1	3.1	3.4
Ta	0.1	0.3	0.5	0.3	0.5	0.2	0.2	0.6	0.5	0.3	0.6	0.7	0.4	0.5
W	<1	6	<1	14	181	<1	<1	160	107	1	201	202	<1	<1
Ir	<5	<5	<5	<5	<5	<5	<5	<5	<5	<5	<5	<5	<5	<5
Au	<2	6	<2	<2	<2	<2	<2	<2	<2	<2	<2	<2	<2	<2
Tl	<0.1	0.1	<0.1	<0.1	0.1	<0.1	<0.1	0.2	<0.1	0.1	0.2	0.2	0.2	0.2
Pb	<5	<5	<5	<5	<5	<5	<5	<5	<5	<5	<5	<5	<5	<5
Bi	<0.4	<0.4	<0.4	<0.4	<0.4	<0.4	<0.4	<0.4	<0.4	<0.4	<0.4	<0.4	<0.4	<0.4
Th	0.2	0.7	1.6	2.5	2.3	1.7	1.3	3.7	5.7	2.8	3.4	3.6	3.7	4.2
U	0.1	0.3	0.6	1	0.9	0.6	0.5	1.3	2.2	1	1.2	1.2	1.3	1.4
Sr/Y	24.92	52.60	37.81	32.59	19.43	26.35	47.06	31.25	14.76	33.44	35.24	34.40	29.29	24.44
La/Yb	3.08	7.15	6.50	7.00	5.90	4.89	7.40	7.82	6.81	7.18	8.22	7.71	7.76	7.83

Table 3 continued

Sample	TV1150	TV1121	TV1147	TV1158	TV1117	TV1116	TV1137A	TV1137B	TV1118	TV1110	TV1146	TV1115	TV1107	
Location	North	3040794	3037089	3039266	3033073	3035902	3035902	3037854	3037854	3036740	3037409	3039273	3035278	3038027
	East	343911	341814	342826	342756	342408	342408	340232	340232	342519	344554	342593	342171	345092
Unit	LVal	Pdcd	Vdcd	Mdld	Mdld	Mdld	Vdld	Vdld, enclave	Vdld	Vdld	UVal	UVal	UVal	
Age	89.8 +9.6/8.8 ka	61 +7/-6.7 ka	51 +8.7/-8 ka	46.0 +3.2/-2.7 ka	46.0 +3.2/-2.7 ka	46.0 +3.2/-2.7 ka	41 +6/-5.8 ka	-	41 +6/-5.8 ka	41 +6/-5.8 ka	22 - 25 ka	22 - 25 ka	22 - 25 ka	
Major Elements (wt. %)														
SiO <sub>2</sub>	60.83	65.94	66	65.89	66.45	64.4	64.48	59.91	66.69	66.23	58.79	57.94	59.83	
Al <sub>2</sub> O <sub>3</sub>	16.42	15.39	15.37	15.94	14.72	15.62	15.62	16.21	15.02	15.61	17.77	17.31	16.99	
Fe <sub>2</sub> O <sub>3</sub>	5.22	5.04	4.75	4.67	3.08	4.28	5.37	6.95	4.55	4.49	6.51	6.67	6.52	
MnO	0.086	0.085	0.082	0.082	0.067	0.078	0.092	0.112	0.079	0.077	0.106	0.11	0.104	
MgO	2.23	1.97	1.88	1.51	0.85	1.56	2.2	2.98	1.81	2.03	3.68	3.87	3.4	
CaO	5.08	4.43	3.9	3.99	2.79	4	4.97	6.45	4.13	4.36	6.99	7.21	6.29	
Na <sub>2</sub> O	4.4	4.26	4.08	4.79	4.79	4.75	4.18	4	4.2	4.28	4.19	4.04	4.23	
K <sub>2</sub> O	1.74	2.05	2.15	2.12	2.38	2.01	1.87	1.27	2.23	2.23	0.91	0.84	1.3	
TiO <sub>2</sub>	0.837	0.751	0.715	0.753	0.588	0.738	0.827	1.06	0.707	0.697	0.998	1.018	1.075	
P <sub>2</sub> O <sub>5</sub>	0.2	0.14	0.12	0.18	0.14	0.17	0.17	0.17	0.15	0.16	0.18	0.19	0.21	
LOI	1.18	0.92	1.49	0.94	2.03	1.36	0.86	0.66	0.32	0.76	0.29	0.81	0.13	
Total	98.21	101	100.5	100.9	97.89	98.98	100.6	99.78	99.88	100.9	100.4	100	100.1	
Trace elements (ppm)														
Be	1	1	1	2	2	1	1	< 1	1	1	< 1	< 1	1	
S	0.121	0.012	0.008	0.001	0.067	0.003	0.005	0.01	0.008	0.064	0.006	< 0.001	0.033	
Sc	11	11	10	9	7	10	12	16	11	11	17	18	16	
V	121	105	95	93	50	94	117	168	99	108	154	159	155	
Cr	< 20	< 20	20	< 20	< 20	< 20	< 20	< 20	< 20	20	50	50	50	

Co	10	10	9	8	32	25	12	17	9	8	34	38	16
Ni	8	18	15	11	2	6	15	17	11	12	33	33	32
Cu	12	16	11	14	4	10	15	14	16	18	28	28	31
Zn	64	56	55	66	58	62	59	66	53	52	67	65	65
Ga	17	16	16	17	16	17	16	17	16	16	17	17	17
Ge	1	1	2	1	1	1	2	1	1	1	1	1	1
As	<5	<5	<5	<5	<5	<5	<5	<5	<5	<5	<5	<5	<5
Se	<3	<3	<3	<3	<3	<3	<3	<3	<3	<3	<3	<3	<3
Br	<0.5	<0.5	<0.5	<0.5	<0.5	<0.5	<0.5	<0.5	<0.5	5.1	<0.5	<0.5	<0.5
Rb	28	44	48	39	48	38	36	21	49	50	12	10	26
Sr	638	318	311	471	347	465	326	374	357	372	469	458	412
Y	17	18	17	21	23	20	19	19	18	20	17	18	22
Zr	130	141	136	191	205	185	128	106	154	161	108	114	171
Nb	4	4	5	6	6	6	4	3	5	5	3	3	5
Mo	3	4	4	6	<2	<2	3	3	3	4	<2	<2	3
Ag	0.5	<0.3	<0.3	0.6	0.5	0.7	0.3	<0.3	<0.3	0.3	0.4	0.4	0.5
Cd	<0.5	<0.5	<0.5	<0.5	<0.5	<0.5	<0.5	<0.5	<0.5	<0.5	<0.5	<0.5	<0.5
In	<0.2	<0.2	<0.2	<0.2	<0.2	<0.2	<0.2	<0.2	<0.2	<0.2	<0.2	<0.2	<0.2
Sn	2	2	3	4	2	2	3	2	2	2	2	1	2
Sb	<0.5	<0.5	<0.5	<0.5	<0.5	<0.5	<0.5	<0.5	<0.5	<0.5	<0.5	<0.5	<0.5
Cs	1.1	1.9	1.9	1.5	1.8	1.4	1.6	1	1.2	1.6	<0.5	0.5	1.2
Ba	545	556	559	579	649	569	506	384	591	580	362	349	414
La	13.8	13.1	13	17.1	18.9	17.1	12.6	9	15.7	16	8.8	9	11.7
Ce	31.3	28.4	27.9	37.5	40.9	37.4	27.2	21	33.6	33.5	20.8	21.4	28.2
Pr	3.68	3.31	3.2	4.41	4.75	4.4	3.2	2.68	3.78	4.16	2.66	2.77	3.56
Nd	15.1	13.2	12.5	17.4	18.8	17.8	13.3	11.8	14.3	16.8	12	12.1	15.4
Sm	3.1	3.2	2.8	3.6	3.9	3.9	3.1	3.1	3.1	3.7	2.9	3.1	3.8
Eu	0.88	0.8	0.76	0.97	0.97	0.97	0.84	0.96	0.78	0.89	0.96	0.99	1.01
Gd	2.9	3	2.8	3.4	3.8	3.7	3	3.3	3.1	3.5	3.2	3.2	3.8
Tb	0.5	0.5	0.5	0.6	0.6	0.6	0.5	0.6	0.5	0.6	0.5	0.5	0.6
Dy	2.8	3.1	2.8	3.4	3.7	3.4	3.1	3.3	2.9	3.4	3	3	3.7

Ho	0.6	0.6	0.6	0.7	0.8	0.7	0.7	0.7	0.6	0.7	0.6	0.6	0.8
Er	1.6	1.9	1.8	2.1	2.3	2.1	1.9	1.9	1.8	2	1.8	1.8	2.2
Tm	0.25	0.28	0.27	0.31	0.36	0.31	0.29	0.28	0.28	0.3	0.27	0.27	0.33
Yb	1.7	1.9	1.9	2.2	2.4	2.2	2	1.9	1.9	2.2	1.8	1.8	2.2
Lu	0.26	0.32	0.3	0.36	0.39	0.35	0.32	0.31	0.31	0.35	0.29	0.29	0.35
Hf	3.1	3.4	3.4	4.4	4.6	4.3	3.4	2.8	3.7	3.9	2.6	2.6	3.9
Ta	0.3	0.4	0.5	0.5	0.9	0.7	0.4	0.3	0.5	0.5	0.4	0.4	0.4
W	<1	<1	<1	76	249	168	<1	2	1	<1	147	178	1
Ir	<5	<5	<5	<5	<5	<5	<5	<5	<5	<5	<5	<5	<5
Au	<2	6	<2	<2	<2	<2	<2	<2	<2	<2	<2	<2	<2
Tl	0.1	0.2	0.2	0.2	0.2	0.2	0.2	0.1	0.2	0.1	<0.1	<0.1	0.2
Pb	<5	<5	<5	<5	8	<5	<5	<5	6	6	<5	<5	<5
Bi	<0.4	<0.4	<0.4	<0.4	<0.4	<0.4	<0.4	<0.4	<0.4	<0.4	<0.4	<0.4	<0.4
Th	2.5	4	4.6	3.8	4.6	3.6	3.4	1.8	4.7	5	1.1	1	2.2
U	0.9	1.4	1.6	1.3	1.6	1.3	1.2	0.7	1.6	1.7	0.5	0.4	0.9
Sr/Y	37.53	17.67	18.29	22.43	15.09	23.25	17.16	19.68	19.83	18.60	27.59	25.44	18.73
La/Yb	8.12	6.89	6.84	7.77	7.88	7.77	6.30	4.74	8.26	7.27	4.89	5.00	5.32

*Highlights*

- The Tres Vírgenes Volcanic Complex lies along a left-lateral fault system caused by a transtensional stress regime.
- The ~300 ka Tres Vírgenes Volcanic Complex emplaced  $39 \text{ km}^3$  of magma over an area of  $120 \text{ km}^2$ .
- The volcanic complex has emitted andesitic to dacitic magmas from 300 to 22 ka.
- Shallow intrusive bodies located about  $>1.2 \text{ km}$  deep could provide a potential geothermal source.



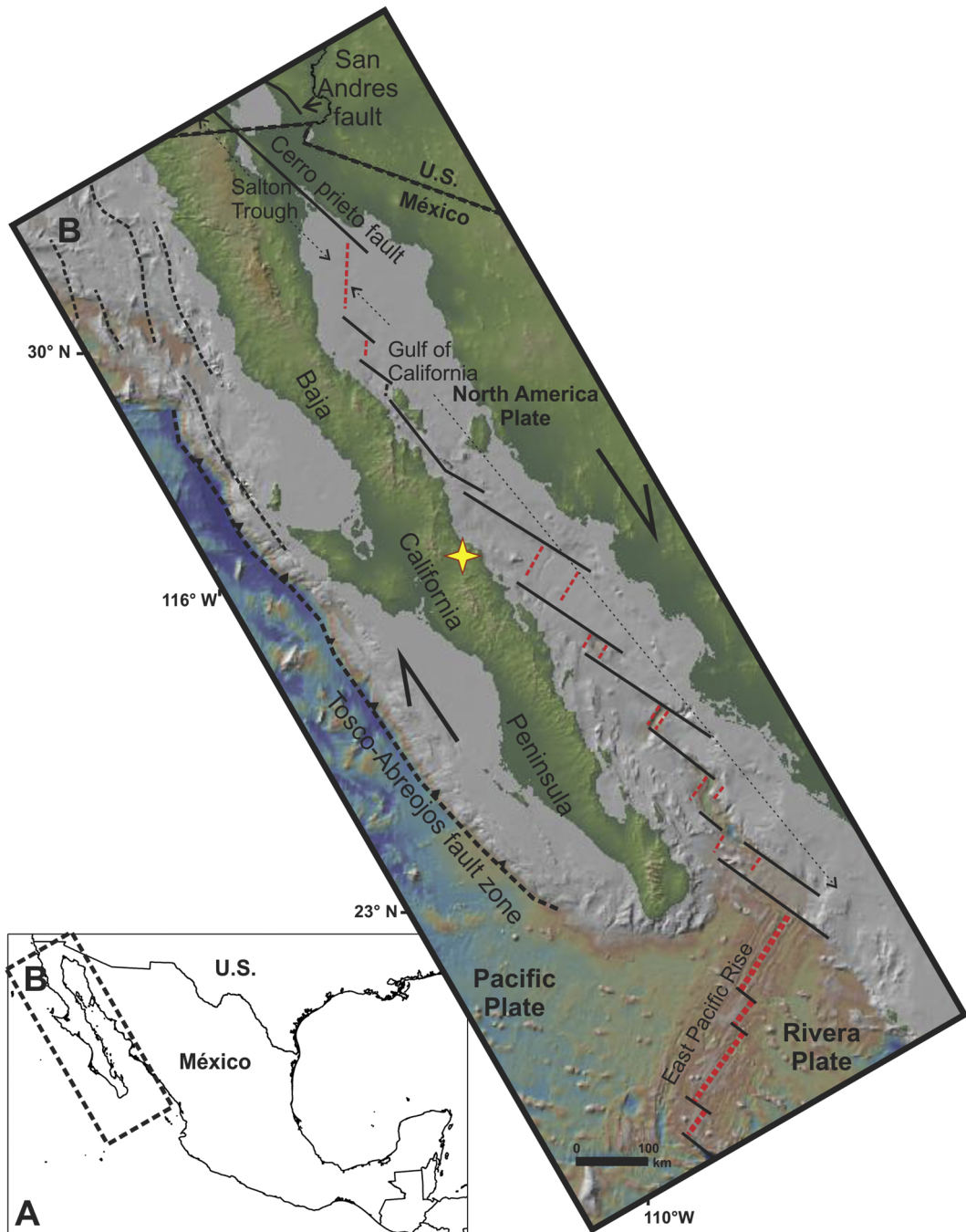
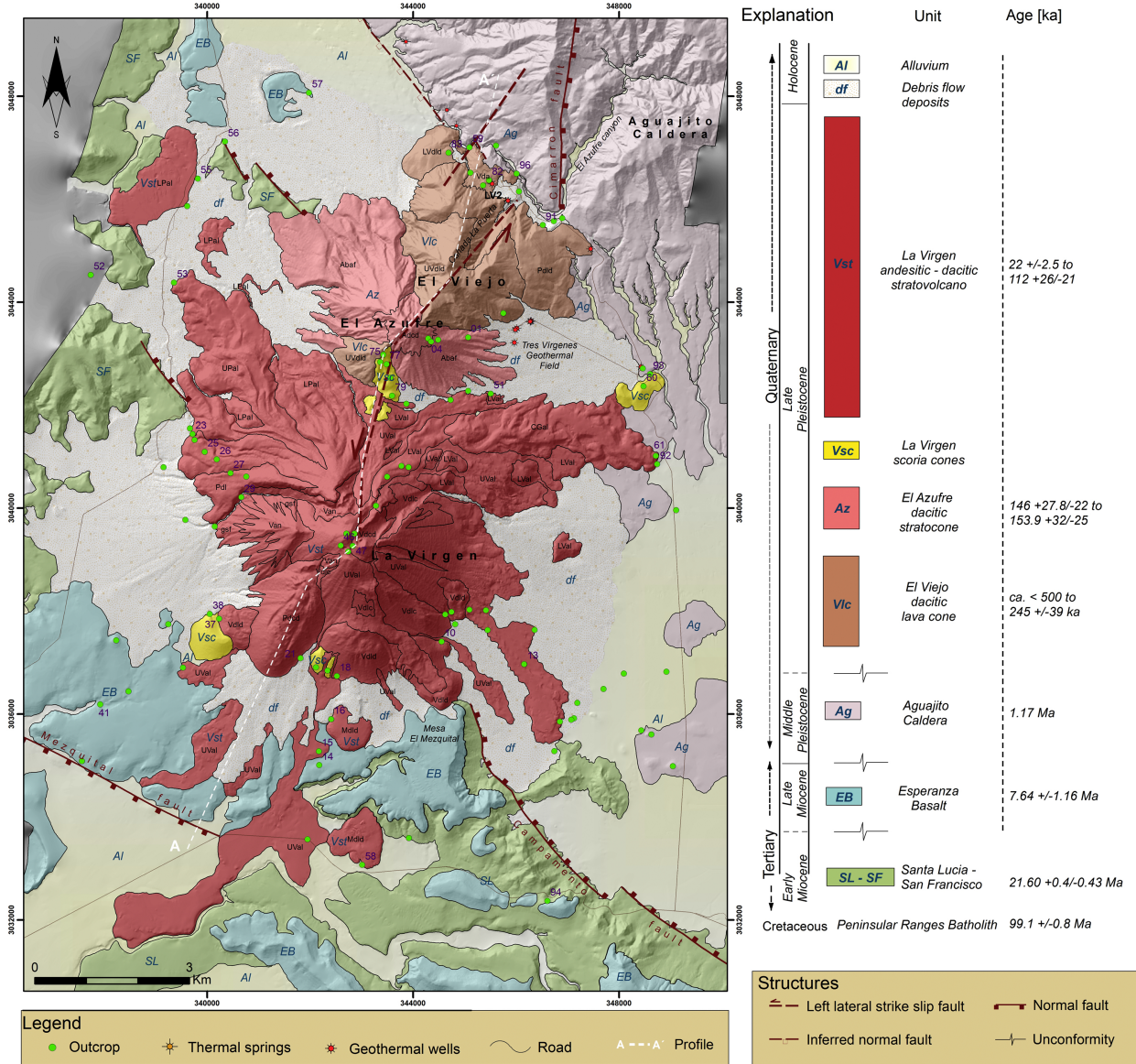


Figure 1





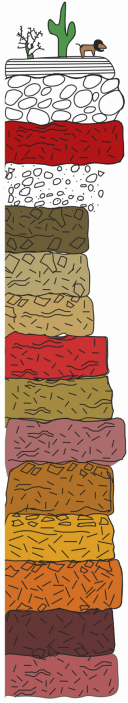



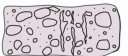
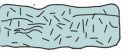


Key used on map	Volcanic structures	Composite stratigraphic column	Description of lithostratigraphic units	Volcanic evolution		
Vst	La Virgen stratovolcano		<p>Al (Alluvium)</p> <p>Dfd (Debris flow deposits)</p> <p>Uval (Upper Virgen andesitic lava; 22 +/-2.5 - 25.5 +/-4.4 ka ): This is a AA lava flow with rough clinker and spine-like (spinose) surface. Rocks are dark-gray to black, moderately vesicular, dominantly aphanitic to porphyritic with plagioclase, orthopyroxene, clinopyroxene and olivine phenocrysts. Lava fragments host pinkish subrounded porphyritic enclaves.</p> <p>VT (Virgen Tephra; 30.7 +/-1.8-1.4 ka): It is a dark-gray to pink, massive, class-supported pyroclastic pumice fall (ca. 83% angular pumice).</p> <p>Vdd (Virgen dacitic lava domes; 41 +/-6/-5.8 ka): Massive lava flows with entablature structures, rocks are porphyritic dark-gray to pinkish-gray with alkali feldspar, amphibole and orthopyroxene phenocrysts. Aphanitic dark-brown enclaves are hosted in these rocks.</p> <p>Mold (Mezquital dacitic lava domes; 46 +/-3.2/-2.7 ka): Light-gray lava flow with a blocky lava surface and crumple breccias exposed at the base of the lava flow fronts.</p> <p>Vdcd (Virgen dacitic central dome; 51 +/-8.7/-8 ka): Lava dome with columnar jointing and a blocky surface containing subrounded, pinkish-gray enclaves. The rock is porphyritic dark-gray lava with plagioclase, amphibole and pyroxene phenocrysts.</p> <p>Pdod (Pinto dacitic coulée dome; 61 +/-7/-6.7 ka): Massive light-gray lava with angular porphyritic blocks made of alkali alkali feldspar and amphibole phenocrysts.</p> <p>Pdi (Pintos dacitic lava; 89.6 +/-11.9/-10.7 ka): Massive lava flows with entablature structure individual blocks have planar curved faces. Rock fragments porphyritic, light-gray with alkali feldspar, plagioclase and amphibole phenocrysts.</p> <p>Lval (Lower Virgen andesitic lava; 89.8 +/-9.6/-8.8 ka): Lava flow with a rough clinkery and spine-like (spinose) surface. Rocks are dark-gray to light-gray, porphyritic with plagioclase and orthopyroxene phenocrysts. Subrounded pinkish-gray porphyritic enclaves with alkali feldspar and amphibole phenocrysts are hosted in the rock.</p> <p>Vdlic (Virgen dacitic lava cone; 102 +/-30/-23.8 ka): Massive dark-gray porphyritic lava flows and autobreccias with alkali feldspar and amphibole phenocrysts.</p> <p>Upal (Upper Pintos andesitic lava; 103.8 +/-12/-11 ka): Light-gray lava flow with entablature structure and detached polyhedral blocks displaying planar curved faces. The rock is porphyritic with plagioclase, clinopyroxene and orthopyroxene phenocrysts.</p> <p>LPal (Lower Pintos andesitic lava; 110.6 +/-43/-30.9 ka): Massive or chaotic blocky lava flows with lava mounds at the surface similar to hornitos; angular lava fragments have detached polyhedral blocks with planar or slightly curved faces and conspicuous dihedral angles. The rock has a scoriaceous porphyritic crust with plagioclase and orthopyroxene.</p> <p>Van (Virgen andesitic neck): Massive reddish to yellowish-gray lava flow with entablature structure limited by blocky lava; rocks are aphanitic to porphyritic with plagioclase and pyroxene phenocrysts.</p> <p>Cgal (Cueva de Gel andesitic lava; 112 +/-26/-21 ka): Massive blocky lava flow bounded by basal and upper autobreccias; the rock is dark-gray, porphyritic with plagioclase, clinopyroxene and orthopyroxene phenocrysts.</p>	<p>two unusual explosive and effusive eruptions sourced at the southwest flank and central vent of La Virgen, respectively</p> <p>fissural effusive eruptions occurred 3 km to the lower southern flanks of La Virgen</p> <p><b>Eruptive epoch 4</b> Construction of the La Virgen stratovolcano that consists of least 13 lithologic units emplaced between 114 and 22 ka through dominantly effusive andesitic eruptions. This stratovolcano was constructed at an average eruptive rate 0.35 km<sup>3</sup>/kyr.</p> <p>fissural effusive eruption occurred on the northeastern lower hillside of the La Virgen</p>		
		Vsc	Virgen scoria cones		<p>surface of subaerial erosion</p> <p>Vsc (Virgen scoria cones): It consist of at least six scoria cones scattered around the La Virgen volcano. The cones consist of massive, clast-supported and poorly sorted fallout beds. Each bed is made of reddish-brown to black, aphanitic scoria lapilli, highly vesicular bombs, and reddish-white to ochre, angular phaneritic enclaves with quartz, alkali feldspar, clinopyroxene and amphibole phenocrysts.</p>	<p>volcanic quiescence plus shifting of active vents</p> <p><b>Eruptive epoch 3</b> Strombolian eruptions occurring at isolated independent vents around the TVVC forming scoria cones</p>
		Az	El Azufre stratocone		<p>surface of subaerial erosion</p> <p>Adod (Azufre dacitic central dome; 153.9 +/-32/-25 ka): Lava dome with crude columnar jointing with angular to subrounded lava blocks with dark-gray enclaves. Lava fragments are dark-gray to pinkish-gray porphyritic with alkali feldspar, quartz and pyroxene phenocrysts.</p> <p>Abaf (Azufre block and ash flow; 146 +/-27.8/-22 ka): Massive, monolithic, matrix-supported block-and-ash flow deposit with angular blocks set in a crumbly medium ash matrix. Light to dark-gray porphyritic blocks contain alkali feldspar, pyroxene and quartz phenocrysts, and subrounded dark-gray aphanitic enclaves with vesicular textures.</p>	<p>volcanic quiescence plus shifting of active vents</p> <p><b>Eruptive epoch 2</b> Construction of the El Azufre stratocone by at least two lithologic units originated between 153 and 130 ka ago through dacitic effusive and explosive eruptions. This stratocone was built at an average eruptive rate 0.084 km<sup>3</sup>/kyr.</p>
		Vlc	El Viejo lava cone		<p>surface of subaerial erosion</p> <p>Vda (Viejo debris avalanche; 245 +/-39 ka): Massive or chaotic, matrix-supported debris avalanche deposit with shattered blocks. Blocks are light-gray with a mottled structure due to abundant subrounded dark-gray enclaves. Some Vda exposures contain abundant clays due to hydrothermal alteration and fumaroles.</p> <p>Uvldd (Upper Viejo dacitic lava dome; 254 +/-24 ka): Lava dome with crude columnar structure and a blocky lava surface. The lava flow is massive with subrounded pink-gray enclaves. Light-gray porphyritic rock with alkali feldspar, amphibole, quartz and pyroxene phenocrysts.</p> <p>Pddd (Puerta dacitic lava dome): This lava flow is massive and contains subrounded 10 cm-sized enclaves. Light-gray porphyritic rock with alkali feldspar, quartz and pyroxene phenocrysts. Enclaves are light-gray with aphanitic texture.</p> <p>Lvldd (Lower Viejo dacitic lava dome): Massive light-gray lava dome with a mottled aspect due to abundant enclaves. Porphyritic rock with alkali feldspar, amphibole and quartz phenocrysts. Dark-gray aphanitic enclaves have different shapes and 5-10 cm-sized diameters.</p>	<p>surface of volcano collapse plus shifting of active vents</p> <p><b>Eruptive epoch 1</b> Construction of the El Viejo lava cone made of three lithologic units emplaced between ca. 300 and 245 ka, formed by dacitic effusive eruptions. This lava cone was built at an average eruptive rate 0.076 km<sup>3</sup>/kyr.</p>
		Ag	Aguajito caldera		<p>surface of subaerial erosion</p> <p>Ag (Aguajito ignimbrite; 1.17 Ma): Massive, matrix-supported welded ignimbrite with lapilli to block pumice, flammé, and lithic fragment set in a fine ash matrix.</p>	<p>structural hiatus and volcanic quiescence</p> <p>post-subduction volcanism</p>
		EB	Esperanza Basalt		<p>surface of subaerial erosion</p> <p>EB (Esperanza Basalt; 7.64 +/-1.16 Ma): Dark-gray lava with the surface covered by reddish-brown pigments; the rock is porphyritic with plagioclase and olivine phenocrysts and large vesicles.</p>	<p>tectonic hiatus and therefore volcanic quiescence</p> <p>volcanism related to rifting associated to the opening to the Gulf of California</p>
		SL	Santa Lucia Range		<p>surface of subaerial erosion</p> <p>SL (Santa Lucia; 21.6 Ma): Massive or chaotic beds containing subrounded and angular lava fragments embedded in a welded fine ash matrix; porphyritic gray-pink and red lava fragments contain alkali feldspar, amphibole and quartz phenocrysts. The matrix has the same constituents.</p>	<p>tectonic hiatus and therefore volcanic quiescence</p> <p>volcanism related to subduction</p>
		PRB	Peninsular Ranges Batholith		<p>PRB (Peninsular Ranges Batholith; 99.1 +/-0.8 Ma): Pinkish-white to rare greenish-gray crystalline phaneritic rock with medium-grained crystals (0.4-0.8 cm) of alkali feldspar, biotite, amphibole and quartz.</p>	

Figure 3

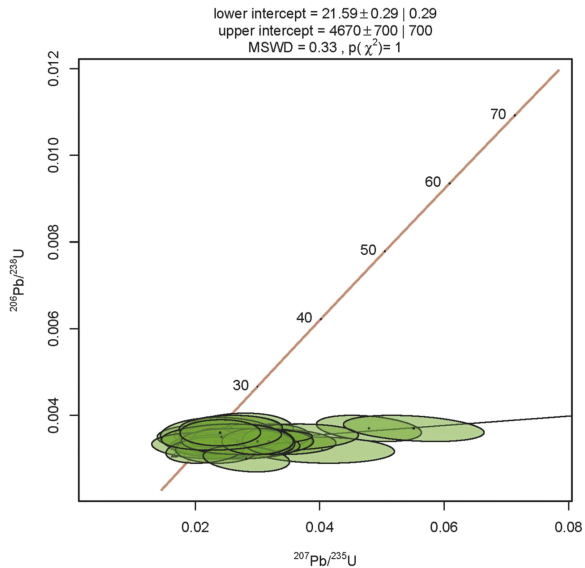
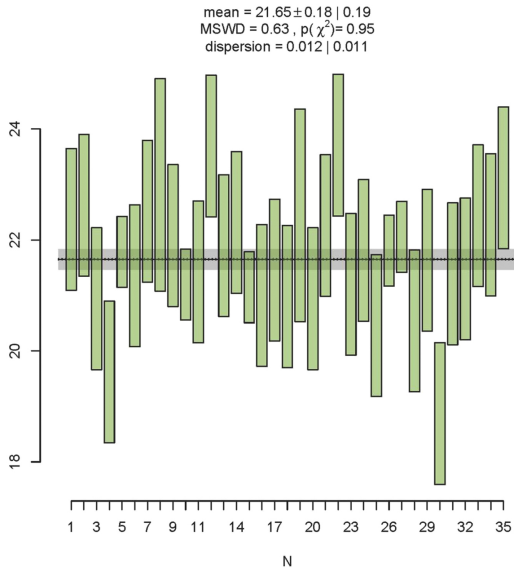


Figure 4

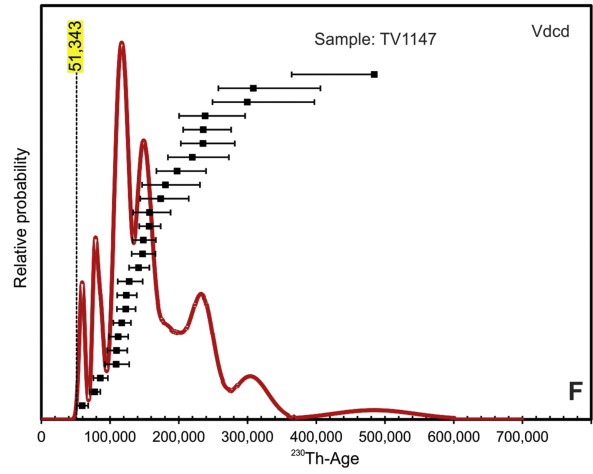
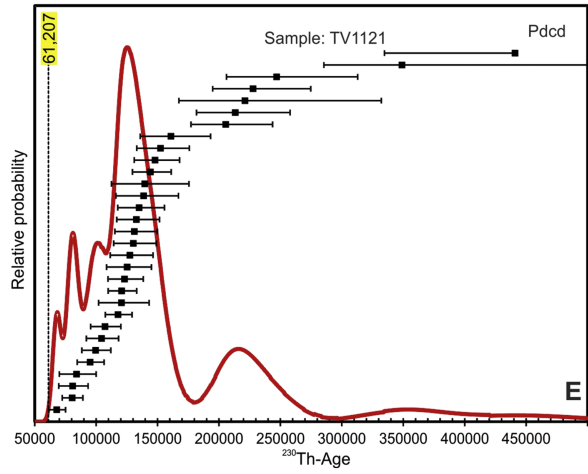
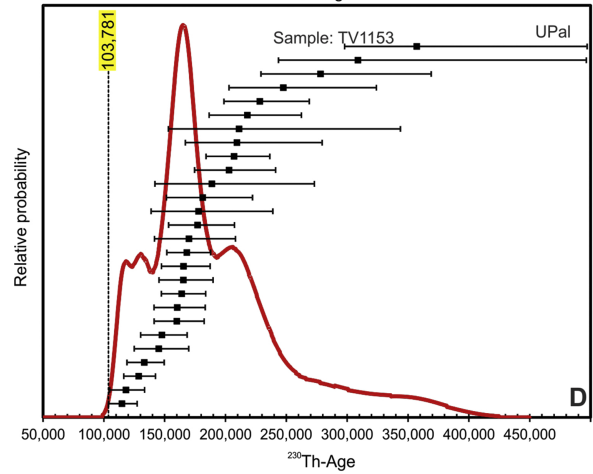
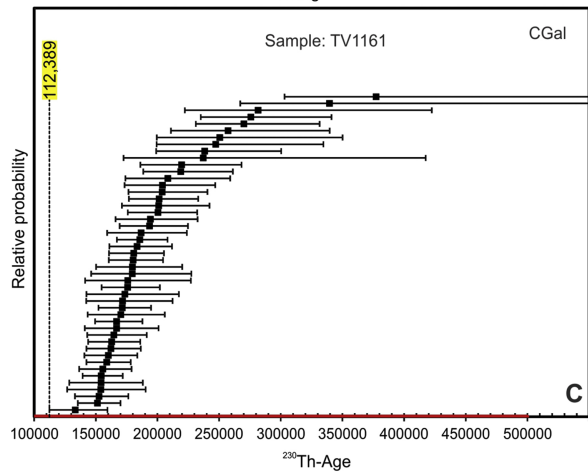
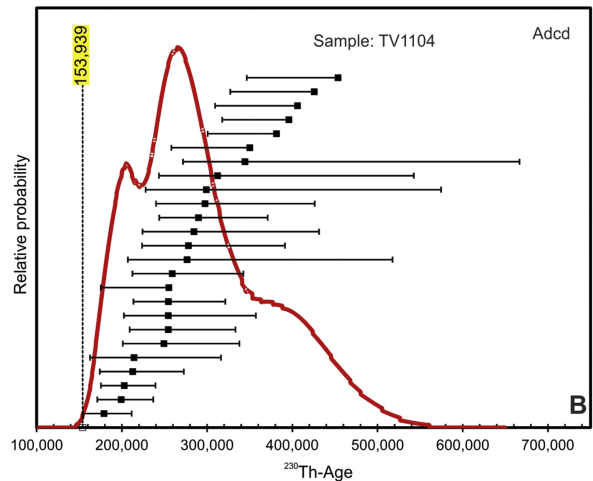
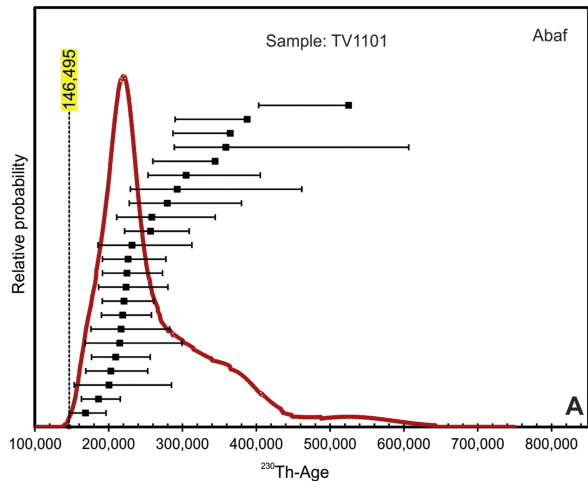
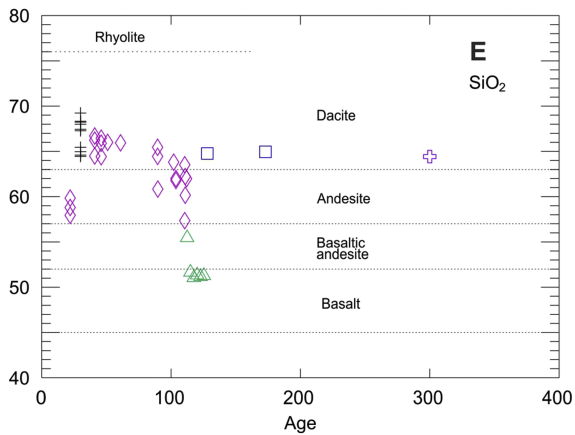
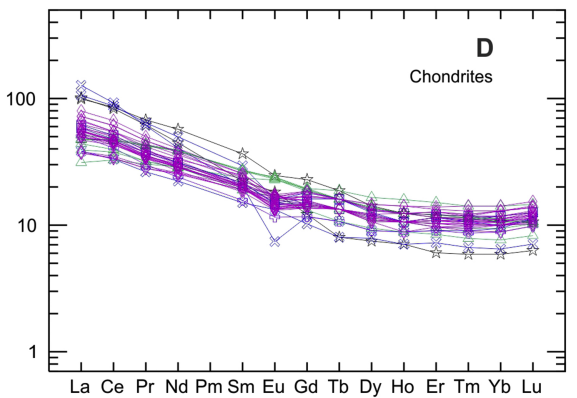
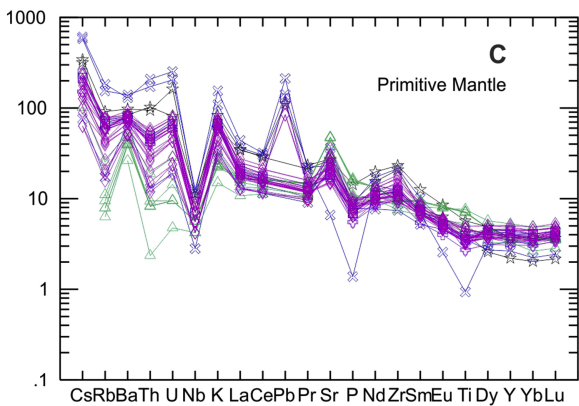
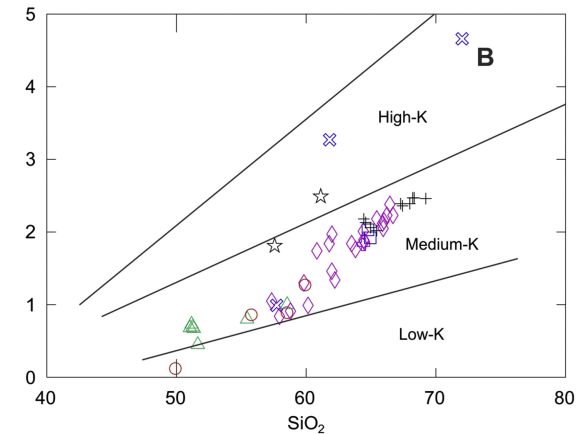
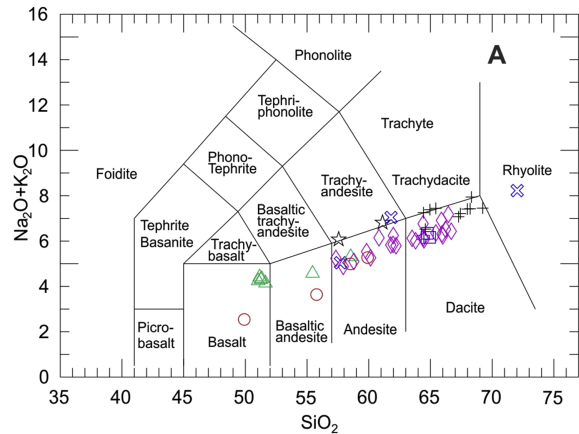


Figure 5



- Symbols
- ◇ La Virgen stratovolcano
  - El Azufre stratocono
  - ⊕ El Viejo lava cone
  - △ La Virgen scoria cones
  - Enclaves
  - ⊗ Santa Lucia
  - ☆ Peninsular Ranges Batholith
  - + La Virgen Tephra

Figure 6



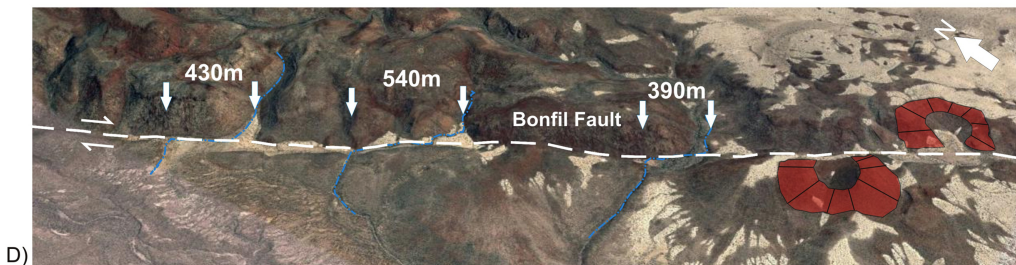
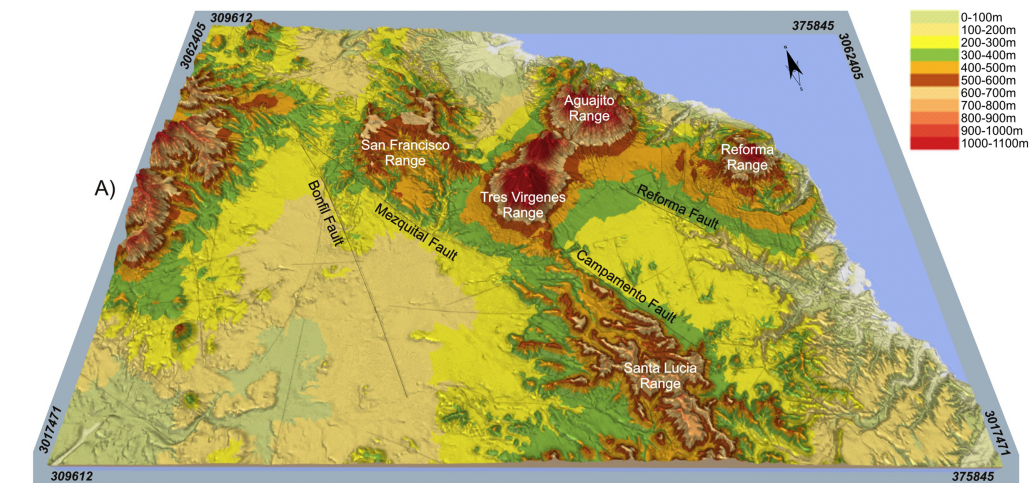


Figure 7



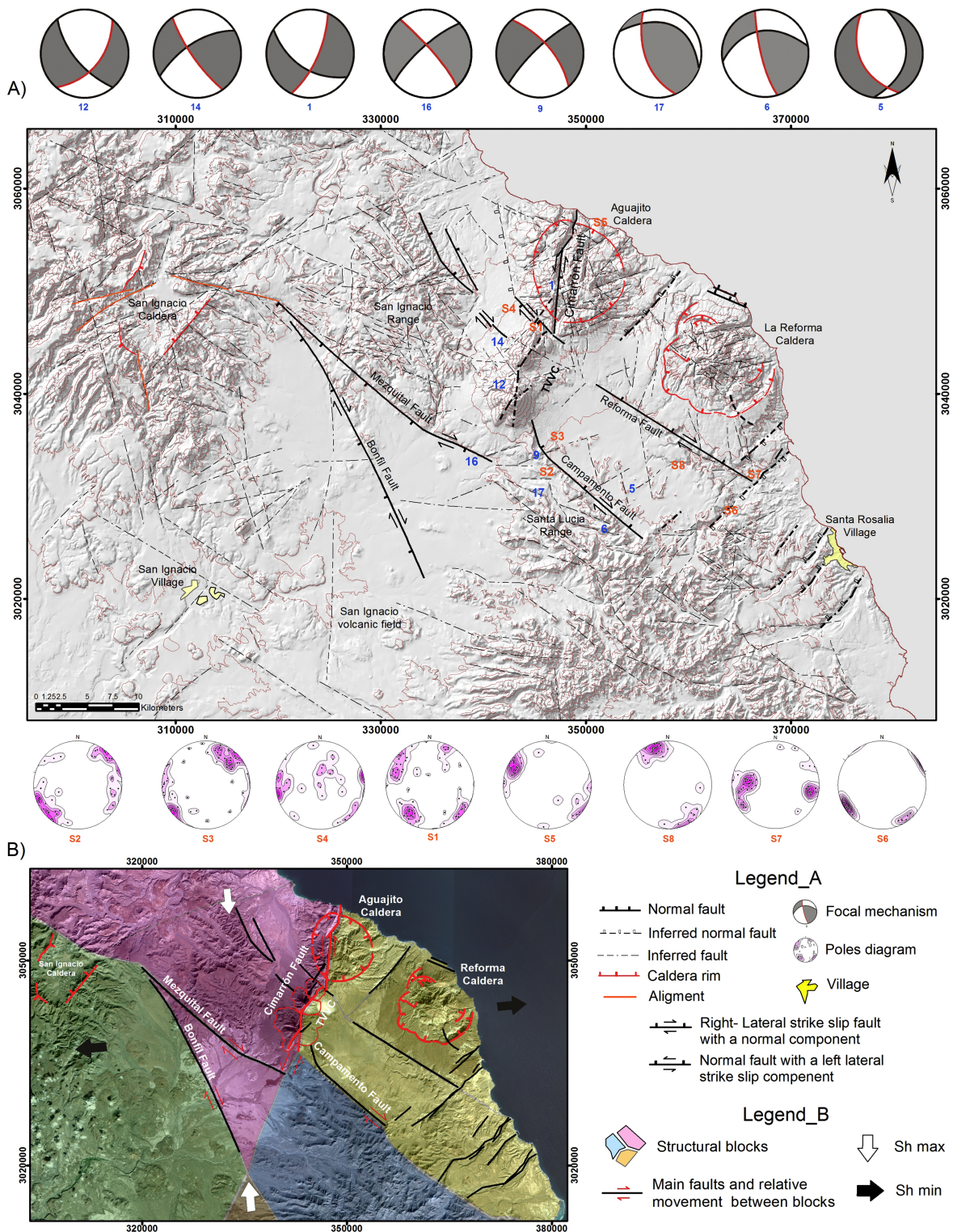


Figure 8



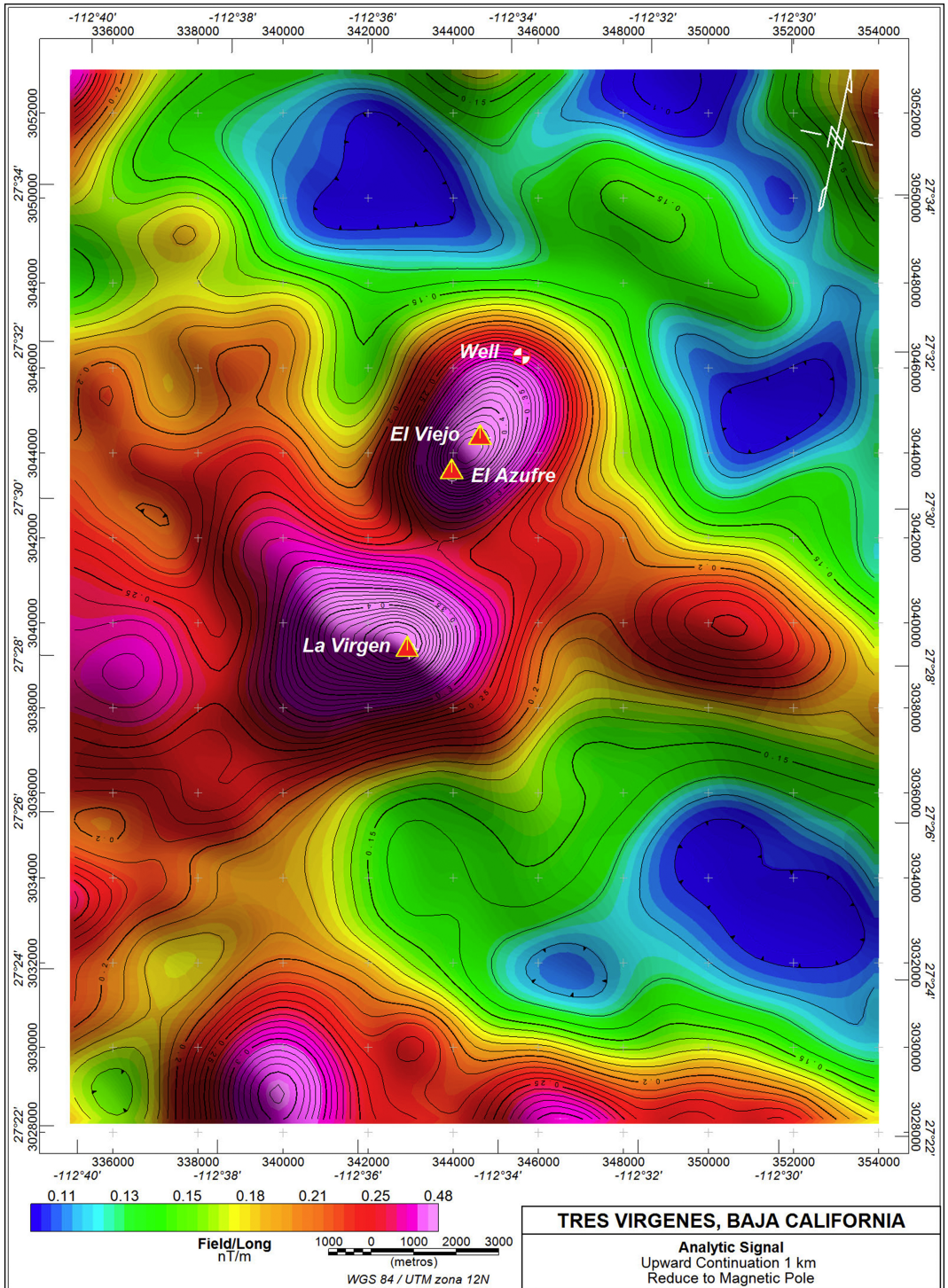


Figure 9

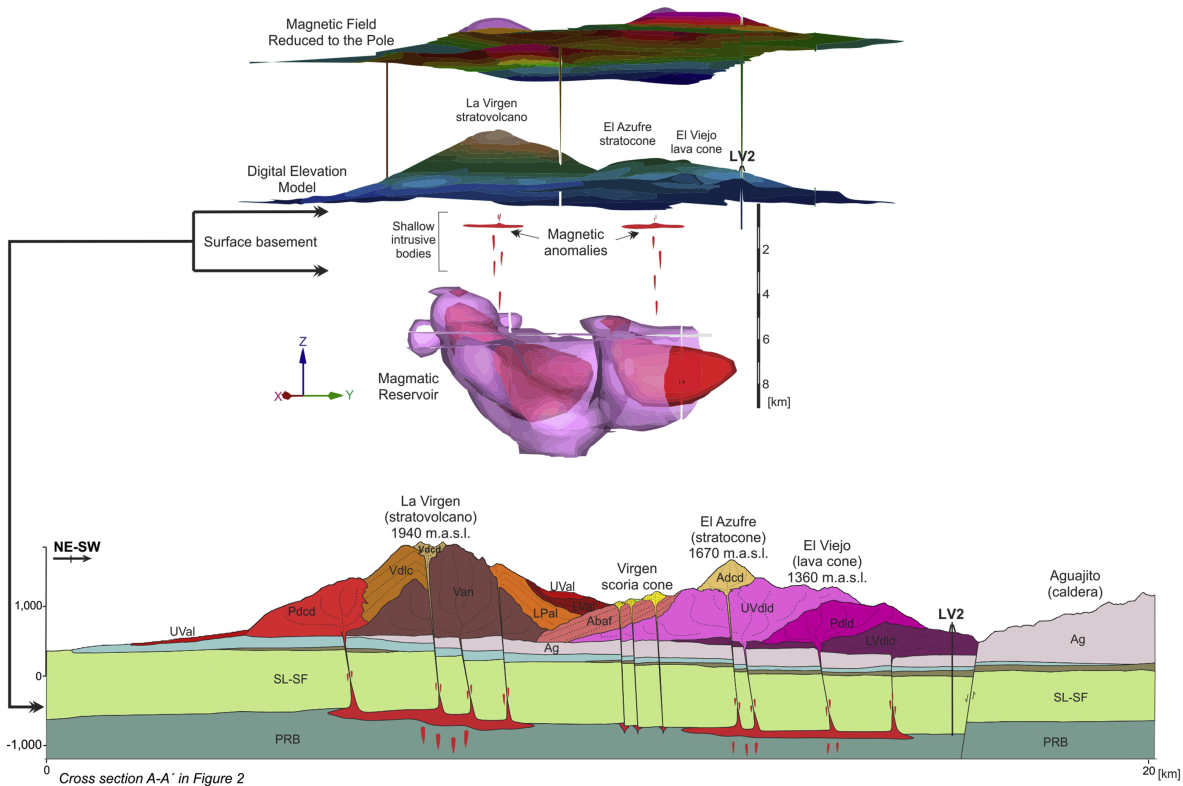


Figure 10

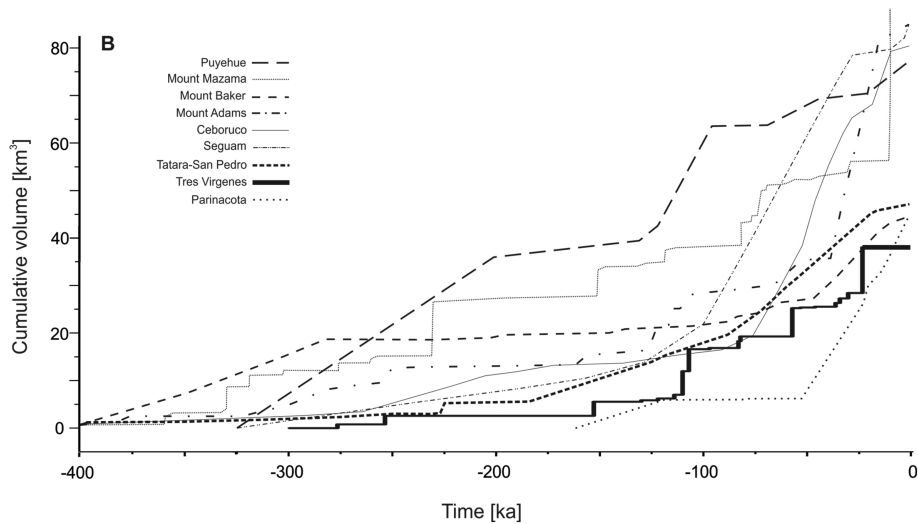
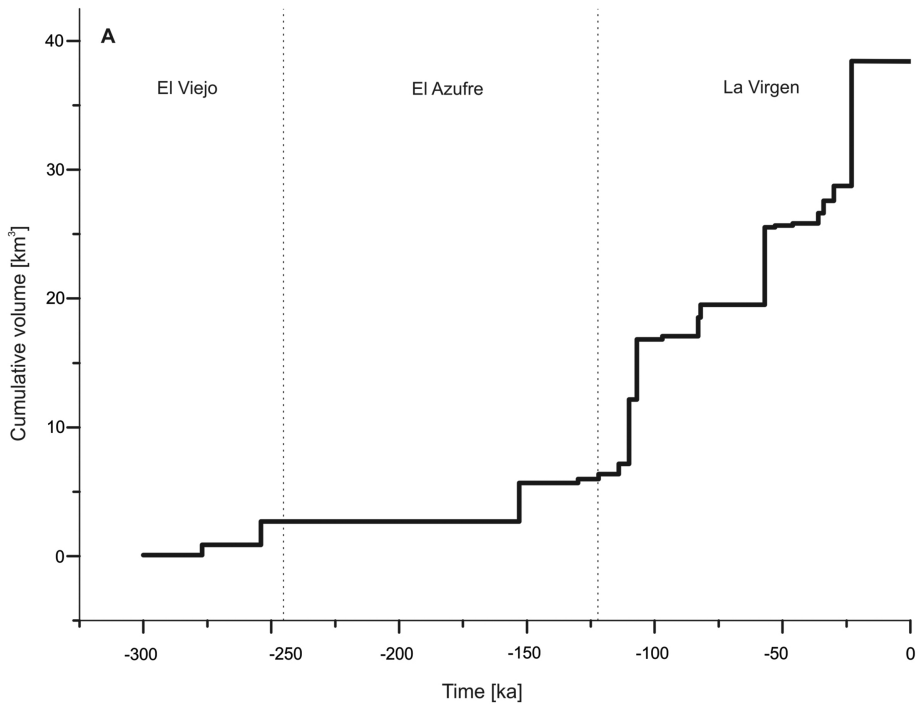


Figure 11